

Last Call for RHIC Predictions

S.A. Bass¹, M. Bleicher², W. Cassing³, A. Dumitru⁴, H.J. Drescher⁵, K.J. Eskola⁶, M. Gyulassy⁷, D. Kharzeev⁸, Y.V. Kovchegov⁹, Z. Lin¹⁰, D. Molnar⁷, J.Y. Ollitrault¹¹, S. Pratt¹², J. Rafelski¹³, R. Rapp¹⁴, D.H. Rischke¹⁵, J.B. Schaffner¹⁵, B.R. Schlei¹⁶, A.M. Snigirev¹⁷, H. Sorge¹⁴, D.K. Srivastava¹⁸, J. Stachel¹⁹, D. Teaney¹⁴, R. Thews¹³, S.E. Vance⁷, I. Vitev⁷, R. Vogt²⁰, X.N. Wang²⁰, B. Zhang¹⁰, J. Zimányi²¹

¹ Physics Dept., Duke Univ., Durham, NC, USA, ² Inst. Theor. Phys., J.W. Goethe Univ., Frankfurt am Main, Germany, ³ Inst. Theor. Phys., Univ. Giessen, Germany, ⁴ Physics Dept., Yale Univ., New Haven, CT, USA, ⁵ Subatech, Univ. Nantes, France, ⁶ Jyvaskyla Univ., Finland, ⁷ Phys. Dept., Columbia Univ., New York, NY, USA, ⁸ Phys. Dept. and RBRC, Brookhaven National Laboratory Upton, NY, USA, ⁹ Dept. Phys., U. Minn., Minneapolis MN, USA, ¹⁰ Phys. Dept., TAM, College Station, TX, USA, ¹¹ Saclay, France, ¹² Dept. Phys., MSU, East Lansing, MI, USA, ¹³ Dept. Phys., Univ. Arizona, Tucson, NM, USA, ¹⁴ Dept. Phys. and Astr., SUNY at Stony Brook, NY, USA, ¹⁵ RIKEN-BNL Research Center, Brookhaven National Laboratory Upton, NY, USA, ¹⁶ Theor. Div., Los Alamos National Laboratory, Los Alamos, NM, USA, ¹⁷ Moscow State Univ., Nuclear Physics Institute, Moscow, Russia, ¹⁸ Variable Energy Cyclotron Centre, Bidhan Nagar, Calcutta, India, ¹⁹ Dept. Phys., Heidelberg Univ., Heidelberg, Germany, ²⁰ Nucl. Sci. Div., LBNL, Berkeley, CA, USA, ²¹ RMKI, Budapest, Hungary

INTRODUCTION

Post-diction has become an art form at AGS and SPS energies. The timing of QM99, just as the RHIC facility comes on-line after nearly two decades of planning and construction, provides a unique opportunity to break out of that mold. The one day Quark Matter 1999 session, organized by M. Gyulassy, had the goal of updating and documenting the *PRE*-dictions for the upcoming RHIC experiments. Of course, sticking one's neck out just as the experimental "guillotine" starts its descent is risky. The brave participants in this session presented a wide range of predictions summarized in this collection of contributions.

The contributions are organized into five sections: (1) Global and Inclusive Observables that probe entropy production and initial conditions in AA, (2) Hadron Flavor Observables that probe hadro-chemical equilibration and baryon number transport, (3) HBT and Collective Flow Observables that probe the space-time volume of the freeze-out surface of the reaction as well as the equation of state of ultra-dense matter, (4) Jets and Penetrating Rare Probes which are sensitive to the highest density phase of the reaction, and (5) Exotic Possibilities that illustrate some of the more speculative novel phenomena that may be explored at RHIC.

1. GLOBAL AND INCLUSIVE OBSERVABLES

1.1. K.J. Eskola: Lower limits for $\langle E_T \rangle$ and $\langle N_{\text{ch}} \rangle$ from pQCD & hydrodynamics at the central rapidity unit in central Au-Au collisions at RHIC [1,2]

In heavy ion collisions at very high cms-energies the initial, very early particle and transverse energy production at central rapidities is expected to be dominated by multiple production of minijets, i.e. gluons, quarks and antiquarks with transverse momenta $p_T \sim 1...2 \text{ GeV} \gg \Lambda_{\text{QCD}}$ [3]. Assuming independent multiple semi-hard parton-parton collisions, the average transverse energy carried by the minijets produced with $p_T \geq p_0$ at the central rapidity window $\Delta y = 1$ in a central ($\mathbf{b} = \mathbf{0}$) AA-collision can be computed in the lowest order (LO) perturbative QCD (pQCD) as [4]

$$E_{T,\text{pQCD}}^{AA}(\sqrt{s}, p_T \geq p_0, \Delta y, \mathbf{0}) = T_{AA}(\mathbf{0}) \int_{p_0, \Delta y} dp_T dy_1 dy_2 \frac{d\sigma}{dp_T dy_1 dy_2} p_T. \quad (1)$$

The differential cross section above is that of each binary (LO) parton collision,

$$\frac{d\sigma}{dp_T^2 dy_1 dy_2} = \sum_{\substack{ijkl= \\ q, \bar{q}, g}} x_1 f_{i/A}(x_1, Q) x_2 f_{j/A}(x_2, Q) \frac{d\hat{\sigma}^{ij \rightarrow kl}}{d\hat{t}} \quad (2)$$

where the rapidities of the outgoing partons are y_1 and y_2 . The nuclear collision geometry is accounted for by the standard nuclear overlap function $T_{AA}(\mathbf{0}) \sim A^2/\pi R_A^2$. In order to have at least one of the two outgoing partons in each minijet collision in the rapidity window Δy , appropriate kinematical cuts have to be made, see [4–6] for details. We use the GRV94-LO parton distributions [7], and, to consistently include both the x - and the Q -dependence of the nuclear effects in the parton distributions ($f_{i/A}(x, Q) \neq f_{i/p}(x, Q)$), we use the recent EKS98-parametrization [8]. We emphasize that the results presented here are obtained by using merely the lowest order pQCD but in order to approximate the effects of the next-to-leading-order terms in the minijet cross sections, we include K -factors 2.0 (1.5) for RHIC (LHC), together with the scale choice $Q = p_T$.

From saturation arguments [6], and from requiring agreement with inclusive pion spectra at central rapidities in $p\bar{p}$ collisions at $\sqrt{s} = 200 \text{ GeV}$, we expect $p_0 \sim 1...2 \text{ GeV}$ for Au-Au collisions at RHIC. The few-GeV minijets are produced within a short proper time $\tau_i \sim 1/p_0 \sim 0.2...0.1 \text{ fm}/c$, so they serve as initial conditions for further evolution of the early QGP. In addition to the pQCD component, at RHIC we also expect a non-negligible non-perturbative (soft) component in the initial transverse energy production. For the simple estimates here, we take the soft component directly from the measured average E_T at $\eta \sim 0$ at central Pb-Pb collisions at the SPS [9]. The *initial* transverse energy at $\tau = 1/p_0$ thus becomes $E_T^i = E_{T,\text{pQCD}}^{AA} + E_T^{\text{N}A49}$, as shown by the dashed lines in Fig. 1a. Dividing by the initial volume $V_i = \pi R_A^2 \tau_i \Delta y$, we get a Bjorken-estimate of the initial energy density: $\epsilon_i = E_T^i/V_i$. In a fully thermalized, 1+1 dimensional boost-invariant hydrodynamic system, the pdV work causes the energy density to decrease as $\epsilon \sim \tau^{-4/3}$ [10] and, especially, *the transverse energy to decrease* as $E_T \sim \tau^{-1/3}$. We do not attempt to follow the system through a phase transition here but simply decouple the system at $\epsilon_f = 1.5 \text{ GeV fm}^{-3}$. The resulting E_T^{final} represents a lower limit of $\langle E_T \rangle$ (mod the decrease in the mixed/hadronic phase), and is plotted by the solid curves in Fig. 1a. It should also be noted that when transverse expansion is included, the loss of E_T is less than in the 1+1 dimensional case considered above.

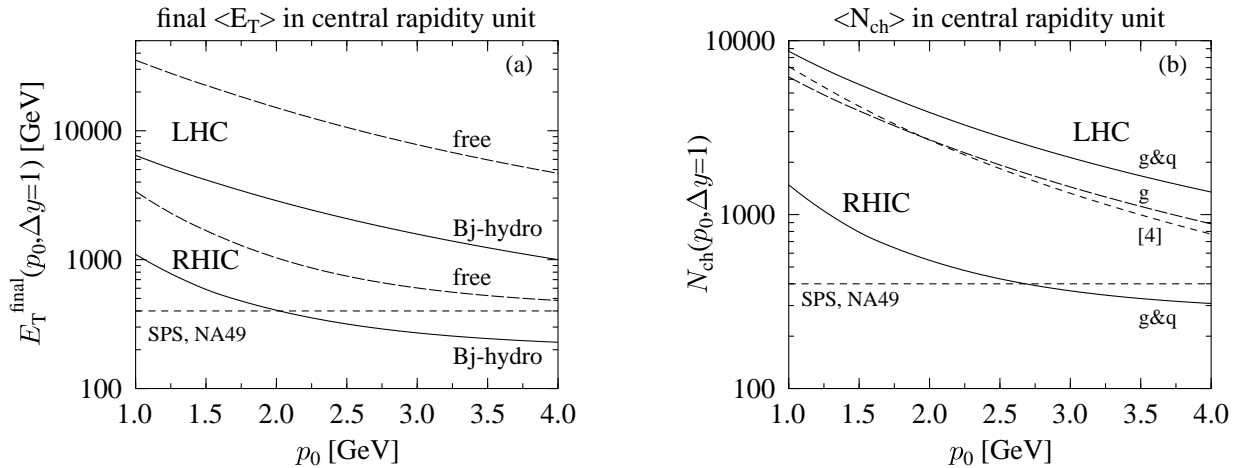


Figure 1. Final $\langle E_T \rangle$ and $\langle N_{ch} \rangle$ in the central rapidity unit.

To get a corresponding estimate of the final state charged pion multiplicity (Fig. 1b), we convert the initial energy density ϵ_i into a temperature T_i , from which the initial rapidity density of entropy S_i can be computed. For simplicity (in spite of gluon dominance), let us assume full thermalization of gluons and quarks here. In an isentropic boost-invariant 1+1 dimensional flow, the rapidity density of entropy is conserved, so $S_i = S_f \approx 4\frac{3}{2}N_{ch}$ [5], where N_{ch} is the final state charged pion multiplicity in the central rapidity unit. In other words, we obtain a lower limit of N_{ch} from entropy of the initial state.

To show the dependence on the transverse momentum cut-off, we plot the lower limits for $\langle E_T \rangle$ and N_{ch} as functions of p_0 (the solid curves). The upper limit of E_T^{final} is the initial E_T^i , so p_0 can be fixed from some other arguments, the measured $\langle E_T \rangle$ serves in principle also as a measure of thermalization. Our favorite estimates for the lower limits can be read off from the figures at $p_0 \sim 1.5$ for RHIC and at $p_0 \sim 2$ GeV for the LHC.

REFERENCES

1. in collaboration with K. Tuominen.
2. <http://www.urhic.phys.jyu.fi/> and <http://www.qm99.to.infn.it/program/qmprogram.html>
3. J.-P. Blaizot and A.H. Mueller, Nucl. Phys. B289 (1987) 847;
K. Kajantie, P.V. Landshoff and J. Lindfors, Phys. Rev. Lett. 59 (1987) 2517.
4. K.J. Eskola, K. Kajantie and J. Lindfors, Nucl. Phys. B323 (1989) 37.
5. K.J. Eskola, K. Kajantie and P.V. Ruuskanen, Phys. Lett. B332 (1994) 191.
6. K.J. Eskola and K. Kajantie, Z. Phys. C75 (1997) 515.
7. M. Glück, E. Reya and A. Vogt, Z. Phys. C67 (1995) 433.
8. K.J. Eskola, V.J. Kolhinen and C.A. Salgado, hep-ph/9807297, Eur. Phys. J. C, in press;
K.J. Eskola, V.J. Kolhinen and P.V. Ruuskanen, Nucl. Phys. B535 (1998) 351.
9. NA49 collaboration, S. Margetis *et al.*, Phys. Rev. Lett. 75 (1995) 3814.
10. J. D. Bjorken, Phys. Rev. D27 (1983) 140.

1.2. Yu.V. Kovchegov: Nuclei and Classical Yang Mills

This contribution is based on the paper [1] in collaboration with A. H. Mueller. The transparencies can be viewed at the web address given in [3].

First let us consider scattering of a gauge invariant current $j = -\frac{1}{4}F_{\mu\nu}^a F_{\mu\nu}^a$ on a nucleus. The single gluon inclusive production amplitude for this process viewed in covariant gauge $\partial \cdot A = 0$ is depicted in Fig. 2. The current (dashed line) interacts with a nucleon in the nucleus producing a gluon, which then rescatters on the other nucleons in the nucleus. The interactions of the propagating gluon with nucleons are pictured in the quasi-classical approximation [1–3]. That limits the interactions to one (inelastic) or two (elastic) gluon exchanges (see Fig. 2) in the eikonal approximation. Interactions involving more gluons are suppressed by the powers of α_s . We consider the case of not very high center of mass energy and not very large transverse momentum of the produced particles, so that there is no large logarithms to enhance those extra powers of α_s . Our expansion is equivalent to resummation in the powers of the effective parameter $\alpha_s^2 A^{1/3}$ [1,2], with A the atomic number of the nucleus.

A calculation outlined in [1] yields for the number of gluons produced at the transverse position x_\perp :

$$\tilde{N}(x_\perp^2) = \int d^2b \frac{N_c^2 - 1}{\pi^2 \alpha N_c x_\perp^2} \left[1 - \exp \left(-\frac{2\pi^2 \sqrt{R^2 - b^2} x_\perp^2 \alpha N_c}{N_c^2 - 1} \rho x G(x, 1/x_\perp^2) \right) \right], \quad (3)$$

where we assumed that the nucleus is a sphere of radius R and has a constant density ρ . The gluon distribution of each nucleon is given by $xG(x, Q^2)$ and is taken at the two-gluon level [1]. We note that in covariant gauge everything is given by the final state interactions, which result in a simple Glauber expression of Eq. (3). If one views the process in the light cone gauge $A_+ = 0$, where the nucleus is moving in the “plus” direction, everything can be pictured in terms of initial state interactions. The nuclear wave function, given by non-Abelian Weizsäcker-Williams field [2], provides us with a gluon which already has all the information about the multiple rescatterings that broaden its transverse momentum. This gluon simply interacts with the current producing a final state on-shell gluon [1]. The resulting production cross section is, of course, the same as given by Eq. (3), since it is a gauge invariant object.

Similar effects happen in the proton-nucleus (pA) collisions. We are just going to state the answer for the total inclusive gluon production cross section in the quasi-classical

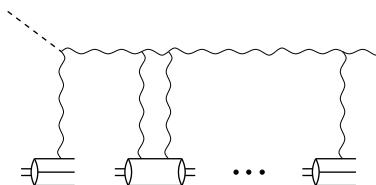


Figure 2. Gluon production in the current-nucleus interaction as envisioned in the text.

approximation [1]:

$$\frac{d\sigma}{d^2l dy} = \frac{1}{\pi} \int d^2b \left\{ \frac{\partial}{\partial l^2} xG(x, l^2) + xG(x, \langle l_{\perp}^2 \rangle) \frac{e^{-\frac{l^2}{\langle l_{\perp}^2 \rangle}}}{\langle l_{\perp}^2 \rangle} \right\}. \quad (4)$$

Here $\langle l_{\perp}^2 \rangle$ is the typical transverse momentum squared of the produced gluon [1]. Formula (4) has a very simple physical interpretation: the first term on the right hand side corresponds to the gluon emission off the proton after the proton passes through the nucleus and the second term provides us with gluon's transverse momentum broadening corresponding to the case when the gluon is already present in the proton's wave function before the collision and multiply rescatters on the nucleons in the nucleus during the collision.

Eq. (4) is written for the case of $l^2 \ll \langle l_{\perp}^2 \rangle$. The general formula, which is given in [1] is plotted in Fig. 3 for the case of proton-gold collision, where we assumed a simple superposition form of the gluon distribution function of a nucleon $xG_{p,n} \approx 3xG_q = 3\frac{\alpha_C E}{\Lambda^2} \ln(Q^2/\Lambda^2)$. In Fig. 3 we show the logarithm of the gluon production cross section $\frac{d\sigma}{d^2l dy}$ as a function of the transverse momentum of the gluon l . We put $\langle l_{\perp}^2 \rangle = 2 \text{ GeV}^2$ for RHIC ($\langle l_{\perp}^2 \rangle$ is, in general, energy dependent). At this lowest order the rest of Eq. (4) is energy (and rapidity) independent.

It is a very interesting and challenging problem to calculate the gluon production cross section for the case of nucleus-nucleus collision in the quasi-classical approximation, i.e., resumming all powers of $\alpha_s^2 A^{1/3}$ (strong field limit). Some attempts in that direction have been made already [4]. However they correspond to the weak field limit [1,2]. The full nucleus-nucleus problem is still to be solved.

REFERENCES

1. Yu. V. Kovchegov, A.H. Mueller, Nucl. Phys. **B 529**, 451 (1998).
2. Yu. V. Kovchegov, Phys. Rev. **D 54** 5463 (1996); **D 55** 5445 (1997).
3. <http://www.qm99.to.infn.it/program/qmprogram.html>
4. A. Kovner, L. McLerran, H. Weigert, Phys. Rev. **D 52**, 3809 (1995); Yu. V. Kovchegov, D. H. Rischke, Phys. Rev. **C 56** 1084 (1997).

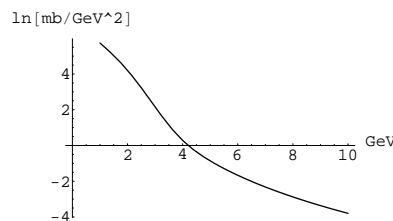


Figure 3. Differential gluon production cross section as a function of gluon's transverse momentum for p+Au collision.

1.3. X.N. Wang: HIJING at RHIC

In this section we will present estimates of hadron spectra in central $Au+Au$ collisions at RHIC energy from perturbative QCD parton models (for high p_T spectra) and HIJING model (for dN_{ch}/dy). Since there are many nuclear effects (including the formation of QGP) which we still don't quantitatively understand, the extrapolation from $p\bar{p}$ data at the RHIC energy and $p+A$, $A+A$ data at SPS energy is inevitably rigged with uncertainties. We will try to estimate these uncertainties by considering different scenarios of various nuclear effects, like nuclear parton shadowing and jet quenching due to parton energy loss in dense matter. For definiteness, central collisions are restricted to events with impact parameters smaller than 3 fm.

Hadron spectra at large transverse momentum in $p\bar{p}$ collisions at collider energy $\sqrt{s} = 200$ GeV have been measured and are consistent with pQCD parton model calculations [1]. The hadron spectra for pp collisions at RHIC energy are expected to be almost the same as $p\bar{p}$ in central rapidity region. Nuclear effects like multiple parton scattering and modification of parton distributions in nuclei will modify the hadron spectra in $p+A$ as data have shown. These observed nuclear effects at energies $\sqrt{s} = 20 - 40$ GeV are well accounted for by including the broadening of initial p_T due to multiple parton scattering and the measured nuclear modification of quark distributions in the pQCD parton model [1]. Extrapolation to RHIC is straightforward with a maximum of uncertainty of about 25% for p_T spectra (normalized to the target nucleons A) at around $p_T = 4$ GeV/c. The uncertainty mainly comes from nuclear shadowing of gluon distribution in nuclei which only becomes important at or above RHIC energy. Such uncertainties are significantly larger in $Au+Au$ collisions as shown by the upper set of curves in Fig. 4 where the ratios

$$R_{AA}(p_T) = \frac{d\sigma_{AA}/dyd^2p_T}{\langle N_{\text{binary}} \rangle dN_{pp}/dyd^2p_T} \quad (5)$$

are plotted and $\langle N_{\text{binary}} \rangle$ is the averaged number of binary NN collisions in $A+A$ collisions from the nuclear geometry. Two different parametrizations[2,3] of the gluon shadowing are used in the calculation. If the leading partons suffer medium-induced energy loss, the spectra ratios will be suppressed as shown by the lower set of curves in Fig. 4. So far, $A+A$ collisions at SPS energy have not shown any indication of energy loss [1], it is difficult to predict quantitatively the parton energy loss dE/dx and that is where the biggest uncertainty in p_T spectra comes from. However, any suppression of the spectra at large p_T will be a clear indication of parton energy loss which will be a direct evidence of early parton thermalization.

The estimate of $dN_{\text{ch}}/d\eta$ in $A+A$ collisions at the RHIC energy is much more uncertain than the high p_T spectra because of the dominance of soft physics involved. Here we use HIJING model [2] which incorporate both string-like soft production mechanism and minijet production. We include both the effect of parton shadowing and jet quenching (parton energy loss or partial thermalization of hard partons). The formation of QGP or the early thermalization of soft partons and the subsequent expansion will add more uncertainty to the estimate of the final observed $dN_{\text{ch}}/d\eta$.

Shown in Fig. 5 are estimates of $dN_{\text{ch}}/d\eta$ from HIJING with different parametrizations of shadowing. Uncertainties due to effect of jet quenching are also shown with or without parton energy loss. Including all these effects, there are an uncertainty of about a factor

of 2 in the final $dN_{\text{ch}}/d\eta$. Taken the value of $dN_{\text{ch}}/d\eta = 2.5$ in $p\bar{p}$ collisions at the RHIC energy and assuming the A -scaling at RHIC energy is the same as at SPS ($PbPb/pp \approx 250$), one has the lowest limit of $dN_{\text{ch}}/d\eta = 550$ consistent with the HIJING's lowest estimate. The clarification of jet quenching from high p_T spectra and of the shadowing from $p + A$ data will help to narrow down the uncertainty and help us to understand the experimental value of $dN_{\text{ch}}/d\eta$.

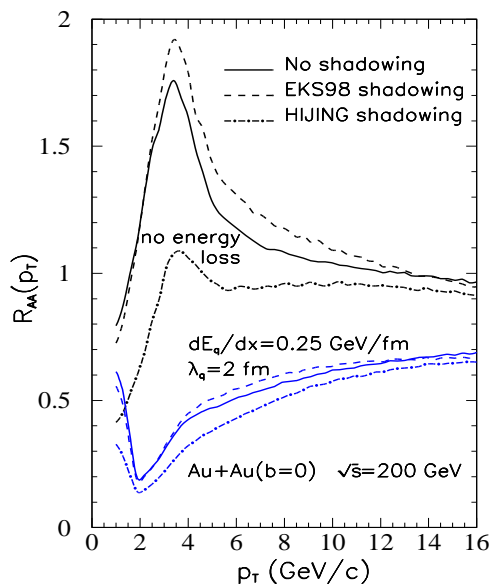


Figure 4. Ratio of hadron spectra in central $Au + Au$ and pp collisions as defined in Eq. 5.

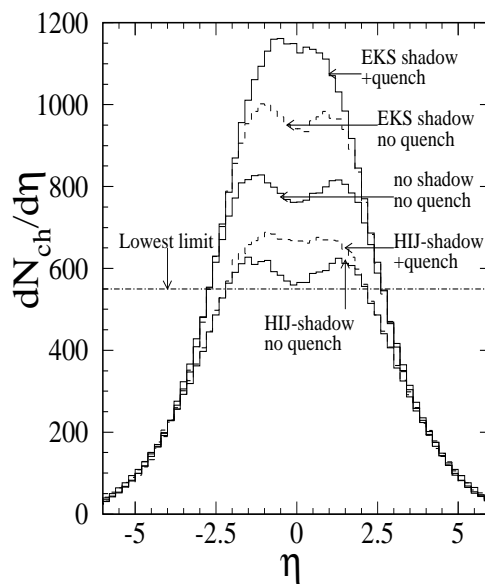


Figure 5. $dN_{\text{ch}}/d\eta$ in central $Au + Au$ collisions. EKS [3] and HIJ [2] parametrizations of parton shadowing are used. $dE/dx = 1$ GeV/fm is used for jet quenching scenario.

REFERENCES

1. X.-N. Wang, Phys. Rev. Lett. **81**, 2655 (1998); nucl-th/9812021
2. X.-N. Wang and M. Gyulassy, Phys. Rev. D **44**, 3501(1991); Comput. Phys. Commun. **83**, 307 (1994).
3. See K. Eskola in this proceedings.

1.4. S.A. Bass: VNI+UrQMD

Transport theory offers the unique possibility to cast the entire time evolution of an ultra-relativistic heavy-ion reaction at RHIC energies – from its initial state to freeze-out – into one consistent framework. In microscopic transport models the full space-time evolution of all microscopic degrees of freedom – either all hadrons present in the system or alternatively (at higher beam energies) partons – is calculated from the initial state to the final freeze-out. At RHIC, the description of the full reaction dynamics from initial state to freeze-out needs to incorporate both, partonic and hadronic, degrees of freedom explicitly in a consistent fashion.

In this contribution [1], a combined microscopic partonic/hadronic transport scenario is introduced: the initial high density partonic phase of the heavy-ion reaction is calculated in the framework of a parton cascade (VNI) [2], using cross sections obtained in the framework of perturbative QCD. The partonic state is then hadronized via a configuration space coalescence and cluster hadronization model and used as initial condition for a hadronic transport calculation using the Ultra-Relativistic-Quantum-Molecular-Dynamics (UrQMD) [3] hadronic transport approach, which has been extensively tested in the AGS and CERN/SPS energy regimes.

The upper left frame of Fig. 6 shows the time evolution (in c.m. time, $t_{c.m.}$) of the rapidity density dN/dy of partons (i.e. quarks and gluons) and on-shell hadron multiplicities at $|y_{c.m.}| \leq 0.5$. Hadronic and partonic phases evolve in parallel and both, parton-parton as well as hadron-hadron interactions occur in the same space-time volume. The overlap between the partonic and hadronic stages of the reaction stretches from $t_{c.m.} \approx 1$ fm/c up to $t_{c.m.} \approx 4$ fm/c for the mid-rapidity region. The calculation indicates that this overlap occurs not only in time but also in coordinate space – partonic and hadronic degrees of freedom occupy the same space-time volume during this reaction phase [4]. Hadronic resonances like the $\Delta(1232)$ and the $\rho(770)$ are formed and remain populated up to $t_{c.m.} \approx 15 - 20$ fm/c, indicating a considerable amount of hadronic rescattering.

Rates for hadron-hadron collisions per unit rapidity at $y_{c.m.}$ are shown in the left lower frame of Fig. 6. Meson-meson and meson-baryon interactions dominate the dynamics of the hadronic phase. Due to their larger cross sections baryon-antibaryon collisions occur more frequently than baryon-baryon interactions.

These hadronic rescatterings influence strongly the m_t -spectra of final state hadrons, e.g. negatively charged hadrons and protons, as can be seen in the right upper and lower frames of Fig. 6. Here calculations with (full circles) and without (open squares) hadronic rescattering are shown: both, the low- m_t as well as the high- m_t domains of the proton spectrum show a depletion due to hadronic rescattering. The proton yield is depleted by baryon-antibaryon annihilations which manifests itself mostly in the low- m_t domain. For h^- , hadronic interactions lead to a depletion in the high- m_t area of the spectrum and to an enhancement in the low- m_t domain. This effect may significantly affect signatures of partonic in-medium physics, like jet-quenching. However, the amount of hadronic rescattering crucially depends on the treatment of hadronization: if hadrons require an *additional* formation time $\tau_f \sim \gamma/M_{had}$ *after* having coalesced from colored constituents into color-neutral hadrons *before* being able to interact, then rescattering effects are strongly suppressed (full triangles).

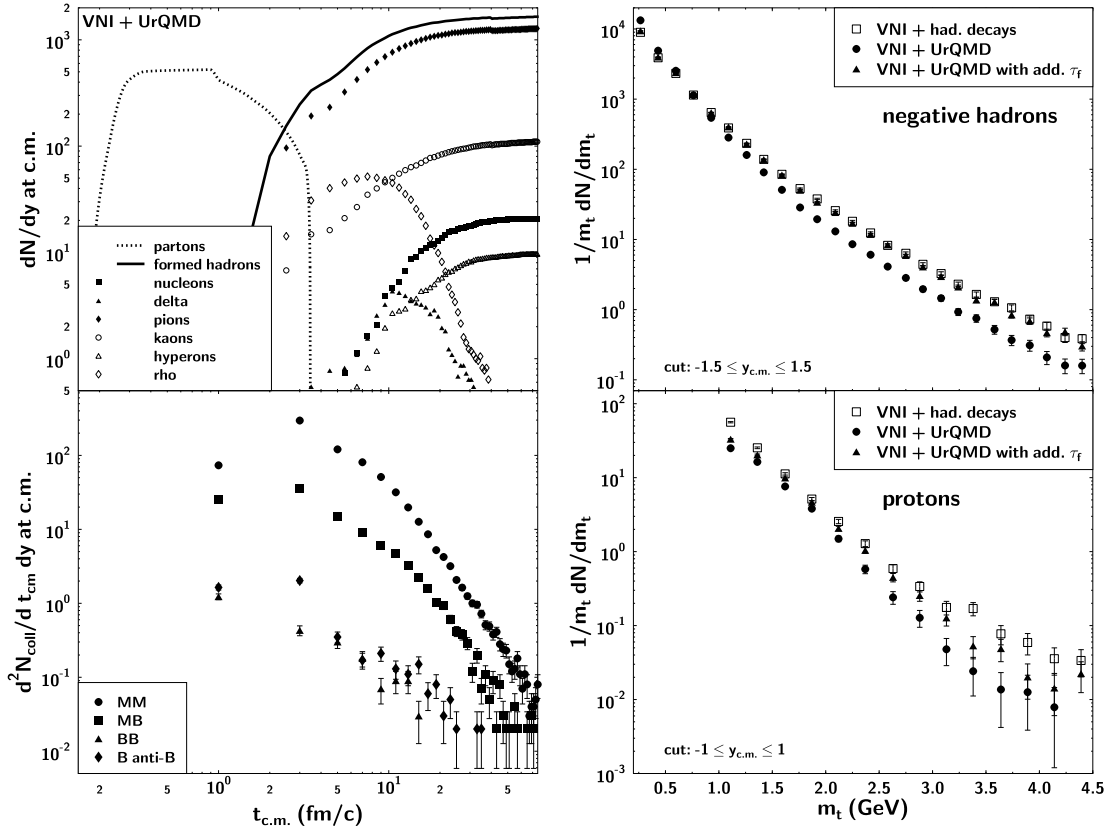


Figure 6. Top left: time evolution of the parton and on-shell hadron rapidity densities at c.m. for central ($b \leq 1$ fm) Au+Au collisions at RHIC. Bottom left: Rates for hadron-hadron collisions per rapidity at c.m. . Right: transverse mass spectra for negatively charged hadrons (top) and protons (bottom) with and without hadronic rescattering.

REFERENCES

1. See also <http://www.phy.duke.edu/~bass/qm99.html>
2. K. Geiger, Comp. Phys. Com. **104** (1997) 70.
3. S.A. Bass *et al.*, Prog. Part. Nucl. Phys. **41** 225 (1998).
4. S.A. Bass, M. Hofmann, M. Bleicher, L. Bravina, E. Zabrodin, H. Stöcker and W. Greiner, Phys. Rev. C in print, eprint nucl-th/9902055.

1.5. A. Dumitru: Hydrodynamics at RHIC

I summarize results for Au+Au at RHIC obtained within hydrodynamics (also combined with a microscopic kinetic model for the late stage). Refs. [1,2] provide more figures and papers, where also references to previous work by others can be found.

The hydrodynamical description of heavy-ion collisions is very appealing because for a given equation of state the (drastic) assumption of local equilibrium uniquely determines the solution within the forward light-cone from the specified initial conditions. Here, an EoS with first-order phase transition between a hadronic phase and a quark-gluon phase is employed, cf. [1] for details. A net baryon and entropy rapidity density of $dN_B/dy = 25$, $dS/dy = 5000$, are employed, as might be appropriate for Au+Au at RHIC. The spectra

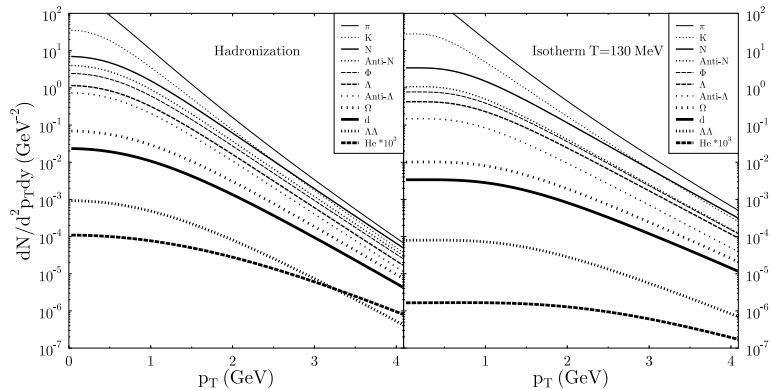


Figure 7. p_T -spectra of various hadrons at hadronization (left) and at $T = 130$ MeV (right) from hydrodynamics w/o final resonance decays (Au+Au at RHIC, $y = 0$, $b = 0$).

of the hadrons on a given hypersurface can be obtained from the well-known Cooper-Frye formula. The p_T -spectra at hadronization and on the $T = 130$ MeV isotherm are shown in Fig. 7. One observes the increasing “stiffness” with the particle mass, i.e. $\langle p_T \rangle$ increases. Also, due to the “hadronic explosion” after hadronization collective flow increases substantially if ideal flow persists even deep in the hadronic phase (which it doesn’t, see below). The work performed by the isentropic expansion (mostly by that of the QGP) reduces the transverse energy per unit of rapidity, dE_T/dy , by 40% (initially it is 1.2 TeV).

In later stages of the reaction the fluid becomes rather dilute and ideal flow breaks down (of course, there may be no region of validity at all). For example, dissipation will increase together with the mean-free paths. Furthermore, one can not determine the freeze-out hypersurface(s) of the various hadron species from ideal hydrodynamics.

A solution to these problems is to chose a suitable hypersurface were to switch from fluid dynamics to a more detailed kinetic theory (e.g. the Boltzmann equation) which explicitly accounts for the various processes between the particles of the fluid. One can then *calculate* self-consistently the freeze-out domains of the various elementary processes as determined by the local expansion rate and the cross-sections of those interactions, and *predict* hadron momentum spectra, two-particle correlators, etc. Since the equilibrium-limit of

the microscopic transport theory is just hydrodynamics, the switch can be performed on any hypersurface within the region of validity of fluid dynamics (the energy-momentum tensors and conserved currents match on the hypersurface).

Calculations have been performed [2] where the switch was done on the hadronization hypersurface. The average collective flow velocity (of π , K , N , Λ) increases from 0.35 at hadronization to 0.4-0.45 at freeze-out. The late hadronic “explosion” is found to be weaker than at SPS, i.e. kinetic freeze-out at RHIC is closer to hadronization and the system cools down less far. In particular, Ξ and Ω baryons, which have small cross sections, decouple shortly after being hadronized and do not gain substantial flow during the hadronic stage. Therefore, the inverse slopes of their m_T -spectra are predicted to be smaller than on the $T = 130$ MeV isotherm, cf. Fig. 8. Another interesting observation is

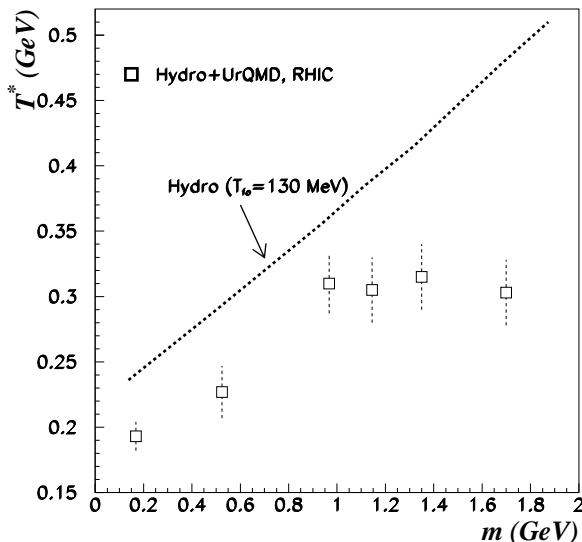


Figure 8. Inverse slopes of various hadron species (Au+Au at RHIC, $y = 0$, $b = 0$) for pure hydrodynamics (on the $T = 130$ MeV isotherm) and for the Hydro+UrQMD model.

that chemical reactions among the most abundant hadron species (π , K , N) are difficult after hadronization, the respective dN/dy 's change by $\leq 20\%$ (besides the contribution from resonance decays). This is because the large expansion rate suppresses inelastic processes, which typically have larger relaxation times than elastic scatterings.

REFERENCES

1. <http://star.physics.yale.edu/theory/>;
A. Dumitru, D.H. Rischke, Phys. Rev. **C59**, 354 (1999)
2. A. Dumitru et al., nucl-th/9901046; S.A. Bass et al., nucl-th/9902062

1.6. H.J. Drescher: NEXUS at RHIC

NEXUS is a model to describe high energy interactions from e^+e^- annihilation up to nucleus-nucleus collisions. The basic physics features (like fragmentation, parton cascading, etc.) are tested and parameters are fixed considering the simplest reaction possible. This reduces possible sources of errors and uncertainties.

Basic interaction mechanism in NEXUS are parton ladders, calculated as a hard scattering with corresponding initial and final state evolution of partons. The initial state radiation is based on a forward evolution algorithm in order to treat consistently energy sharing in multiple scattering.

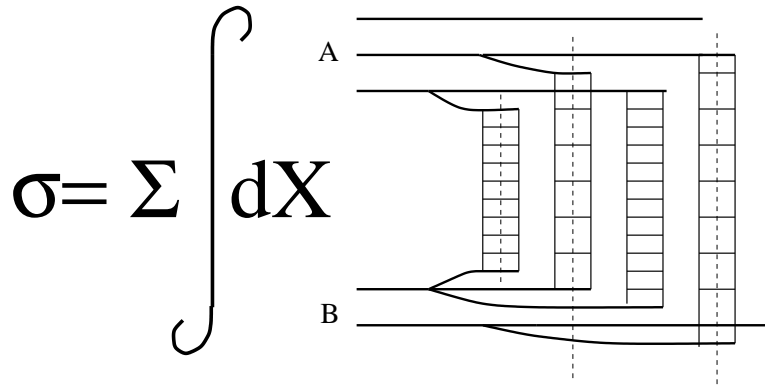


Figure 9. Symbolic representation of the total cross section in NEXUS.

It is important to notice that multiple collisions happen simultaneously and momentum has to be shared among all collisions according to the different contributions to the total cross section. This leads to a complicated formula with a sum over all possible number of cut and uncut parton ladders. To choose one of these configurations in a Monte-Carlo framework is a highly dimensional problem. This is achieved with techniques coming from statistical physics, the Metropolis algorithm and Markov chains. At this stage the algorithm uses some approximations, but a future version of NEXUS will treat this properly.

After primary interactions and particle productions via string decay the rescattering of particles is done. For this, particles follow classical trajectories in a Lorenz invariant frame. According to cross-sections, two particles do an elastic or inelastic scattering. If there are more than two particles close to each other a quark droplet is formed which evolves according to a Bjorken scenario. Dropping below some critical energy density, it decays according to n-dimensional phase space decay. This reproduces well experimentally observed behavior like strangeness enhancement but is based on a theoretically less firm ground.

NEXUS calculations for gold on gold at 200 GeV center of mass energy and an impact parameter less than 2 fm show a charged particle multiplicity of about 1100 particles per rapidity unit in the mid-rapidity region (Fig. 10(a)).

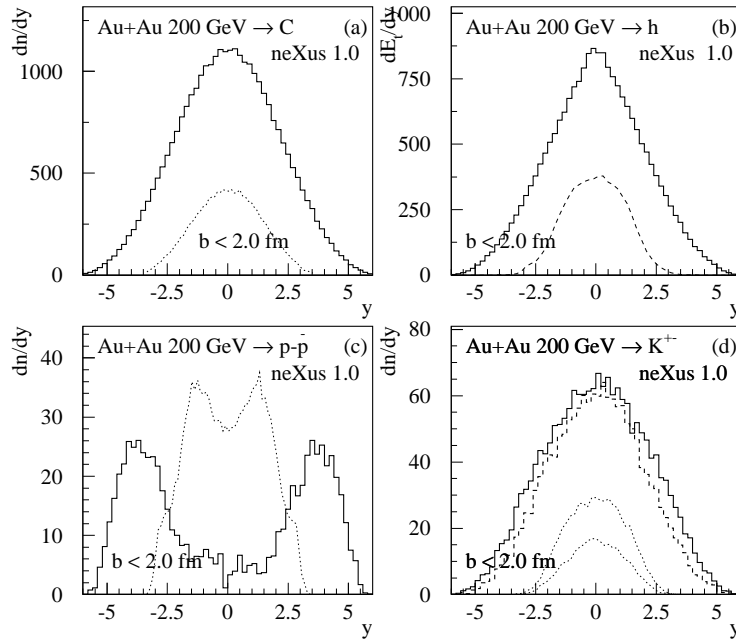


Figure 10. (a) Multiplicity of charged particles (full line) compared to SPS lead-lead (dashed line). (b) Transverse energy dE_t/dy of all particles (full line) compared to SPS (dashed). (c) Rapidity of net protons (full line) compared to SPS results (dashed line). (d) K^+ (full line) and K^- (dashed) and the corresponding SPS results (light dashed lines).

The transverse energy $dE_t/dy|_{y=0}$ of hadrons is about 850 GeV which leads to an energy density of about $7 \text{ GeV}/\text{fm}^3$ (Figure 10(b)). These two observables should have an error bar of about 20% due to approximations in the primary interactions and uncertainties in the rescattering formalism.

More significant should be the result for the rapidity distribution of net protons since it is quite insensitive to secondary interactions. We find a great transparency with a multiplicity of about 5 per rapidity unit at $y = 0$, which means very little stopping power compared to the SPS results (Fig. 10(c)).

Kaons are produced with a multiplicity of about 60 per rapidity unit in the central region (Fig. 10(d)).

More plots can be found in [2].

REFERENCES

1. Hans-Joachim Drescher, Michael Hladik, Serguei Ostapchenko, Klaus Werner
<http://www.qm99.to.infn.it/para16/werner/werner.html>
2. http://www.qm99.to.infn.it/rhic_pred/drescher/drescher.ps.gz
3. <http://www-subatech.in2p3.fr/~theo/nexus>

1.7. H. Sorge: RQMD at RHIC (see in this proceedings)

1.8. M. Bleicher: URQMD at RHIC

As a tool for our investigation of heavy ion reactions at RHIC the Ultra-relativistic Quantum Molecular Dynamics model (UrQMD) is scrutinized. UrQMD is a microscopic transport approach based on the covariant propagation of constituent quarks and diquarks accompanied by mesonic and baryonic degrees of freedom. It includes rescattering of new and produced particles, the excitation and fragmentation of color strings and the formation and decay of hadronic resonances. For further details about the UrQMD model, the reader is referred to Ref. [2]. Note, that these proceedings and the used UrQMD version is based on [3].

The UrQMD model has been applied very successfully to explore heavy ion reaction from below AGS energies (10 AGeV) up to the full CERN-SPS energy (160 AGeV). This includes detailed studies of particle abundances, -spectra, photonic and leptonic probes, J/Ψ 's and event-by-event fluctuations [4].

Let us now start to tackle the relevant questions given to us by the upcoming of the RHIC directly:

- Is a model like UrQMD applicable to AA reactions at RHIC energies?
- What is the predicted amount of baryonic stopping achieved at RHIC?
- How many particles will be produced?
- How strong will the transverse expansion be?

Let me start by answering the first question: It has often been claimed that dual string models fail to describe data above a certain center of mass energy. Let us take a look if this region is reached at RHIC: Comparing the UrQMD predictions to rapidity distributions in He+He at $\sqrt{s} = 31\text{GeV}$ (ISR) leads to a very good description, if we increase to energy further UrQMD starts to deviate from the measured multiplicity data by 35% at $\sqrt{s} = 200\text{GeV}$.

However the collision spectra of individual collisions shows that less than 20% of all reactions belong to this high energy regime ($\sqrt{s} > 100\text{GeV}$). Thus, the remaining 80% of reactions are 'low energetic' and therefore well treatable by string dynamics.

It has been claimed recently, that exotic mechanisms (Baryon junctions) need to be invoked to understand the baryon number transport at SPS and RHIC. In contrast to these approaches the UrQMD model mainly applies quark model cross sections to the subsequent scattering of constituent (di-)quarks in combination with a small diquark breaking component

The stopping power obtained with this approach is rather strong. The net-proton distribution is shifted by more than one unit in rapidity, resulting in approximately 12 net-protons at midrapidity. The stopping of hyperons is even stronger (2 units in rapidity, net- $\Lambda + \Sigma$) leading to a large hyperon density in the central region.

The particle production predicted by the UrQMD approach reaches more than 1100 Pions (750 of them are charged Pions) at midrapidity with approx. 100 additional charged Kaons at midrapidity.

This amount of charged particle abundances at midrapidity is on the lower bound of the expected multiplicity at $y = 0$ which reaches from 600 to 2000. It is interesting to note

that the particle yield is similar to the presented RQMD results and strongly deviates from the reported results obtained by pQCD dominated models.

Let us turn to the transverse expansion created in the UrQMD model. Since the early UrQMD dynamics is based on string degrees of freedom, the newly created quarks are not allowed to interact until they have undergone their coalescence into hadrons (typically this needs 1fm/c in the local rest frame of the coalescing quarks). Due to the large Lorentz γ -factor, this leads to a vanishing pressure in the initial reaction zone. This behaviour is clearly visible in the distribution of the mean transverse momentum as a function of rapidity. A plateau in the $\langle p_{\perp} \rangle(y)$ is observed for the newly created mesons in the central rapidity region - the transverse momenta at $y = 0$ are similar to their pp values. In the case of the Protons a clear dip in the the $\langle p_{\perp} \rangle(y)$ at midrapidity is predicted.

Let me conclude that the semi-hadronic UrQMD model has been applied to Au+Au reactions at RHIC. The use of such an effective model for RHIC may be disputable. However, rigorous QCD predictions (i.e. results which can be directly compared to data to falsify or support this approach) are not available or are even contradicting each other. Therefore it is of utmost importance to use a reliable phenomenological model, like the UrQMD, which has successfully described a large body of measured data at AGS and SPS to investigate the dynamics encountered at RHIC.

REFERENCES

1. **The UrQMD collaboration:** S. A. Bass, M. Belkacem, M. Bleicher, M. Brandstetter, L. Bravina, C. Ernst, L. Gerland, L. Neise, S. Soff, C. Spieles, H. Weber, H. Stöcker, W. Greiner
2. M. Bleicher et al., J. Phys. G 25 (1999)
S. A. Bass et al., Progr. Nucl. Phys. 41 (1998) 225
3. M. Bleicher et al., <http://xxx.lanl.gov/abs/hep-ph/9906398>
4. M. Bleicher et al., Phys. Lett. B 435 (1998) 9
M. Bleicher et al., Phys. Lett. B 447 (1999) 227

1.9. B. Zhang: HIJING+ZPC+ART

To study heavy ion collisions at the Relativistic Heavy Ion Collider (RHIC), we have developed a multi-phase transport model that includes both initial partonic and final hadronic interactions. Specifically, the parton cascade model ZPC [3] is extended to include the quark-gluon to hadronic matter transition and also final-state hadronic interactions based on the ART model [4].

Currently, the ZPC model includes only gluon-gluon elastic scatterings with its cross section taken to be the leading divergent cross section regulated by a medium generated screening mass that is related to the phase space density of produced partons. The input of the parton phase space distribution to the ZPC model is obtained from the HIJING model [5], which includes both hard scatterings via the PYTHIA routines with the nuclear shadowing effect and soft interactions using the Lund soft momentum transfer model. Partons are produced from these scatterings with a formation time determined according to a Lorentzian distribution with a half width given by the ratio of its energy to the square of its transverse mass. The positions of formed partons are then calculated by using straight line propagation from their parent nucleon positions.

Once partons stop interacting, they are converted into hadrons using the HIJING fragmentation scheme after a proper time of approximate 1.2 fm. We consider both the default fragmentation scheme of treating a diquark as a single entity and a modified one which allows the formation of diquark-antidiquark pairs, that fragment into both $BM\bar{B}$ and $B\bar{B}$ with probabilities of 80% and 20%, respectively.

For the hadron evolution, we have used the ART model that includes both elastic and inelastic hadron scatterings. Multiparticle production is modeled through the formation of resonances. Since the inverse double resonance channels have smaller cross sections than those calculated directly from the detailed balance relation, we have adjusted the double resonance absorption cross sections to improve the model.

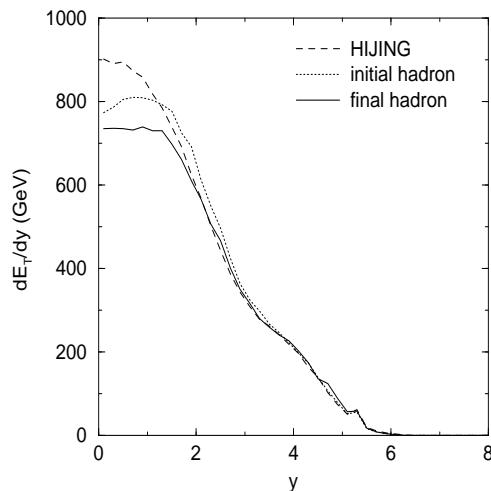


Figure 11. Transverse energy rapidity distribution for central ($b=0$) Au+Au collisions at RHIC.

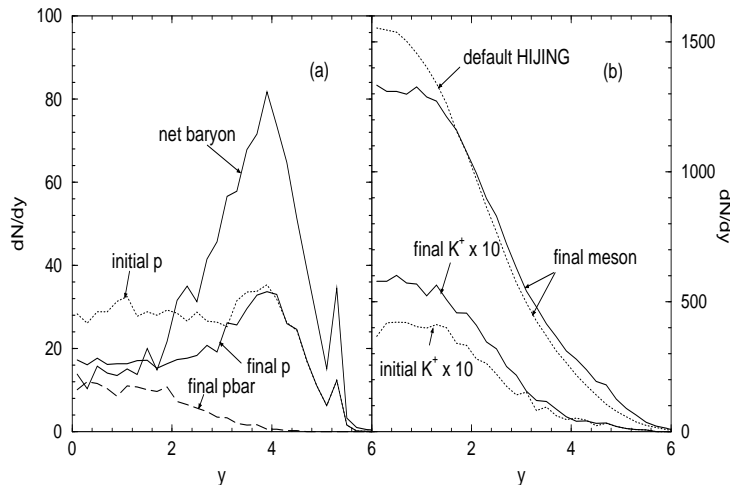


Figure 12. Predictions of (a) baryon and (b) meson rapidity distributions for central ($b=0$) Au+Au collisions at RHIC.

Hadron transverse energy rapidity distributions for RHIC Au+Au central ($b=0$) collisions are shown in Fig. 11. We see that parton evolution and fragmentation lower the distribution by about 100 GeV per unit rapidity while hadron evolution further decreases it by around 50 GeV per unit rapidity. This shows an observable effect of final state interactions. Fig. 12 gives the baryon and meson rapidity distributions. Net baryon distribution has a large rapidity shift due to the modified fragmentation scheme. Many antiprotons are seen to survive the absorption in the hadronic matter, leading to a value of about 10 at central rapidities. The final meson central rapidity distribution shows a distinctive plateau structure. Results using the default HIJING show a similar distribution except that the central rapidity density is higher. Also shown in the figure is the distribution of kaons produced from both string fragmentation and hadronic production. The latter gives significant enhancement of the kaon production.

REFERENCES

1. Talk presented by B.A. Li (in collaboration with C.M. Ko, Z. Lin, and B. Zhang). Work supported by NSF Grant PHY-9870038, Welch Foundation Grant A-1358, and the Texas Advanced Research Project FY97-010366-068. More details in: B. Zhang, C.M. Ko, B.A. Li, and Z. Lin, nucl-th/9904075, to appear in the proceedings of APS Centennial meeting Relativistic Heavy Ion Minisymposium.
2. See <http://www.qm99.to.infn.it/program/qmprogram.html> for transparencies.
3. B. Zhang, Comp. Phys. Comm. 109 (1998) 193; *ibid.* 111 (1998) 276 (E).
4. B.A. Li and C.M. Ko, Phys. Rev. C 52 (1995) 2037.
5. X.N. Wang and M. Gyulassy, Phys. Rev. D 44 (1991) 3501; M. Gyulassy and X.N. Wang, Comp. Phys. Comm. 83 (1994) 307.

1.10. W. Cassing: VNI+HSD

Intuitively one expects that the initial nonequilibrium phase of a nucleus-nucleus collision at RHIC energies should be described by parton degrees of freedom whereas hadrons are only formed (by 'condensation') at a later stage of the reaction which might be a couple of fm/c from the initial contact of the heavy ions. Thus parton cascade calculations [1] – including transition rates from perturbative QCD – should be adequate for all initial reactions involving a large 4-momentum transfer between the constituents since QCD is well tested in its short distance properties. The question, however, remains to which extent the parton calculations can be extrapolated to low Q^2 , where hadronic scales become important, and under which conditions (temperature, quark chemical potential) the expanding system of strongly interacting partons is more appropriately described by an expanding, but interacting hadron gas.

The practical question is, however, if nonequilibrium partonic and hadron/string models can be distinguished at all, i.e. do they lead to different predictions for experimental observables? We will thus compare the predictions from the parton cascade VNI [1] with those from the HSD transport approach [2], which involves quarks, diquarks, antiquarks, antidiquarks, strings and hadrons as degrees of freedom.

We start with pp collisions at $\sqrt{s} = 200$ GeV. The calculated results for the proton, π^+ and K^+ rapidity distributions in the cms are shown in Fig. 13 (upper part) for both models, which are denoted individually by the labels VNI (dashed histograms) and HSD (solid histograms). On the level of pp collisions we find no considerable differences between the two kinetic models with respect to the rapidity distributions for $p, \bar{p}, \pi's$ and K, \bar{K} . This also holds for the p_T spectra.

We directly step towards central collisions ($b \leq 2$ fm) for Au + Au at $\sqrt{s} = 200$ GeV. The calculated results for the proton (here $p - \bar{p}$), antiproton, π^+ and K^+ rapidity distributions in the cms are shown in Fig. 13 (middle part) for both models, which are denoted again by the labels VNI (dashed histograms) and HSD (solid histograms). Here the hadron-string model shows a larger stopping than the parton cascade (l.h.s.) and a flatter distribution in rapidity of antiprotons than the partonic cascade. The pion and kaon multiplicities turn out to be roughly the same, but the results from the parton cascade are more strongly peaked around midrapidity as those from the HSD approach. In physical terms the larger stopping of the HSD approach and the additional production of pions and kaons (relative to pp collisions) stems from secondary and ternary reaction channels in the hadronic rescattering phase, which are quite abundant since the meson densities achieved are very high. The narrow width of the antiproton and meson rapidity distribution (as compared to pp collisions) for VNI is due to an approximate thermalization of the partonic degrees of freedom; in the hadron-string scenario essentially 'comover' scattering occurs with a low change of the meson rapidity distribution. Thus the meson rapidity distributions are practically the same as for pp collisions. Also note that at midrapidity the net baryon density $\sim N_p - N_{\bar{p}}$ is practically zero, however, even at midrapidity a lot of baryons appear that are produced together with antibaryons. Thus also mesons (especially $c\bar{c}$ pairs) will encounter a lot of baryons and antibaryons on their way to the continuum.

In order to demonstrate that the higher baryon stopping, kaon enhancement and widening of the pion rapidity distribution is essentially a rescattering effect, we have extended the parton cascade VNI by the hadronic rescattering phase as described by HSD [2]. The

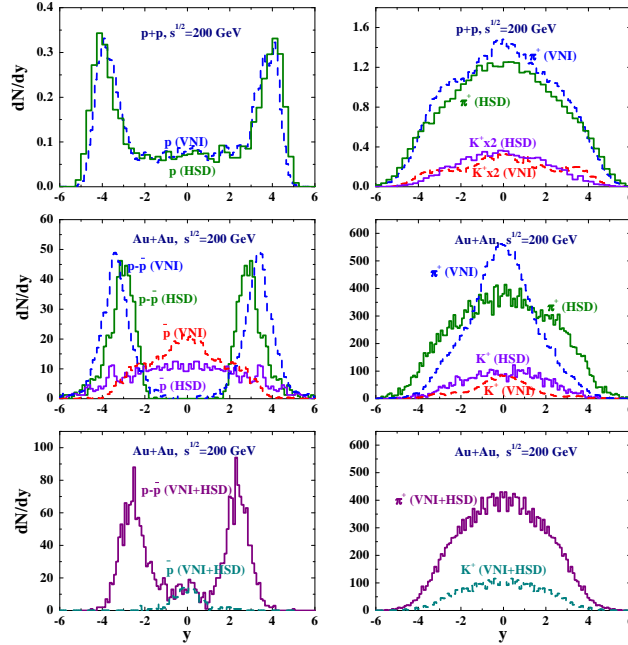


Figure 13. The rapidity spectra of hadrons for pp (upper part) and central collisions of $Au + Au$ at $\sqrt{s} = 200$ GeV within VNI, HSD and VNI + HSD (see text).

results of these calculations (VNI + HSD) for central $Au + Au$ collisions are displayed in the lower part of Fig. 13. It is worth to note that VNI+HSD almost give the same rapidity distributions as HSD which already includes the final state interactions.

We also have performed calculations for low mass dileptons and high mass dimuons [2], where especially the J/Ψ and ψ' peaks are of interest. Without explicit representation we note that in the dimuon spectra – in the 'comover' absorption scenario [3] – the Ψ' peak vanishes almost completely whereas the J/Ψ peak is suppressed by $\approx 90\%$ in central $Au + Au$ collisions due to the high meson densities achieved at these energies.

REFERENCES

1. K. Geiger, Comp. Phys. Commun. 104 (1997) 70.
2. W. Cassing and E. L. Bratkovskaya, Phys. Rep. 308 (1999) 65.
3. W. Cassing and E. L. Bratkovskaya, Nucl. Phys. A623 (1997) 570.

2. HADRONIC FLAVOR OBSERVABLES

2.1. J. Zimányi: Quark Coalescence

There is a possibility, that at RHIC a nice quark gluon plasma will be produced in the collision. This plasma will expand and cool in the next phase. Thus it may happen, that just before the hadronization the same type of matter will be created as in SPS experiments. It is assumed to consist of constituent quark-antiquark matter (CQM) [2,3].

Then the hadronization may proceed via quark coalescence process as described by the ALCOR model just as in the case of SPS. Thus it is worthwhile to make predictions for RHIC assuming coalescence mechanism.

The nonlinear ALCOR coalescence model was created for situations, where the subprocesses are not independent, they compete with each other. In this model the coalescence equations relating the number of a given type of hadron to the product of the numbers of different quarks from which the hadron consists reads as:

$$\begin{aligned}
N_p &= C_p \cdot b_q \cdot b_q \cdot b_q \cdot N_q \cdot N_q \cdot N_q & N_{\bar{p}} &= C_{\bar{p}} \cdot b_{\bar{q}} \cdot b_{\bar{q}} \cdot b_{\bar{q}} \cdot N_{\bar{q}} \cdot N_{\bar{q}} \cdot N_{\bar{q}} \\
N_\Lambda &= C_\Lambda \cdot b_q \cdot b_q \cdot b_s \cdot N_q \cdot N_q \cdot N_s & N_{\bar{\Lambda}} &= C_{\bar{\Lambda}} \cdot b_{\bar{q}} \cdot b_{\bar{q}} \cdot b_{\bar{s}} \cdot N_{\bar{q}} \cdot N_{\bar{q}} \cdot N_{\bar{s}} \\
N_\Xi &= C_\Xi \cdot b_q \cdot b_s \cdot b_s \cdot N_q \cdot N_s \cdot N_s & N_{\bar{\Xi}} &= C_{\bar{\Xi}} \cdot b_{\bar{q}} \cdot b_{\bar{s}} \cdot b_{\bar{s}} \cdot N_{\bar{q}} \cdot N_{\bar{s}} \cdot N_{\bar{s}} \\
N_\Omega &= C_\Omega \cdot b_s \cdot b_s \cdot b_s \cdot N_s \cdot N_s \cdot N_s & N_{\bar{\Omega}} &= C_{\bar{\Omega}} \cdot b_{\bar{s}} \cdot b_{\bar{s}} \cdot b_{\bar{s}} \cdot N_{\bar{s}} \cdot N_{\bar{s}} \cdot N_{\bar{s}}
\end{aligned} \tag{6}$$

$$\begin{aligned}
N_\pi &= C_\pi \cdot b_q \cdot b_{\bar{q}} \cdot N_q \cdot N_{\bar{q}} \\
N_K &= C_K \cdot b_q \cdot b_{\bar{s}} \cdot N_q \cdot N_{\bar{s}} \\
N_{\bar{K}} &= C_{\bar{K}} \cdot b_{\bar{q}} \cdot b_s \cdot N_{\bar{q}} \cdot N_s \\
N_\eta &= C_\eta \cdot b_{\bar{s}} \cdot b_s \cdot N_{\bar{s}} \cdot N_s
\end{aligned} \tag{7}$$

Here the normalization coefficients, b_i , are determined uniquely by the requirement, that the number of the constituent quarks do not change during the hadronization — which is the basic assumption for all quark counting methods:

$$\begin{aligned}
N_s &= 3 \cdot N_\Omega + 2 \cdot N_\Xi + 1 \cdot N_\Lambda + 1 \cdot N_{\bar{K}} + 1 \cdot N_\eta \\
N_{\bar{s}} &= 3 \cdot N_{\bar{\Omega}} + 2 \cdot N_{\bar{\Xi}} + 1 \cdot N_{\bar{\Lambda}} + 1 \cdot N_K + 1 \cdot N_\eta \\
N_q &= 3 \cdot N_p + 1 \cdot N_\Xi + 2 \cdot N_\Lambda + 1 \cdot N_K + 1 \cdot N_\pi \\
N_{\bar{q}} &= 3 \cdot N_{\bar{p}} + 1 \cdot N_{\bar{\Xi}} + 2 \cdot N_{\bar{\Lambda}} + 1 \cdot N_{\bar{K}} + 1 \cdot N_\pi .
\end{aligned} \tag{8}$$

In eq. (8) N_π is the number of directly produced pions. (Most of the observed pions are created in the decay of resonances.) Substituting eqs. (6 - 7) into eq. (8) one obtains equations for the for normalization constants. These constants are then given in terms of quark numbers and C_i factors. However, one can predict some relations even without solving the set of nonlinear equations, eq. (8) [4,5]. Thus one obtains the interesting relations for the antiparticle - particle ratios:

$$\frac{\bar{\Lambda}}{\Lambda} = D \cdot \frac{\bar{p}}{p} , \quad \frac{\bar{\Xi}}{\Xi} = D \cdot \frac{\bar{\Lambda}}{\Lambda} , \quad \frac{\bar{\Omega}}{\Omega} = D \cdot \frac{\bar{\Xi}}{\Xi} ,$$

where $D = K^+/K^-$ (see details in Ref. [5]). At SPS energy the measured value is $D = 1.8 \pm 0.2$ [8] which agrees within the experimental errors with $D = 1.95$ obtained in ALCOR. Our prediction for RHIC energy is $D = 1.2$.

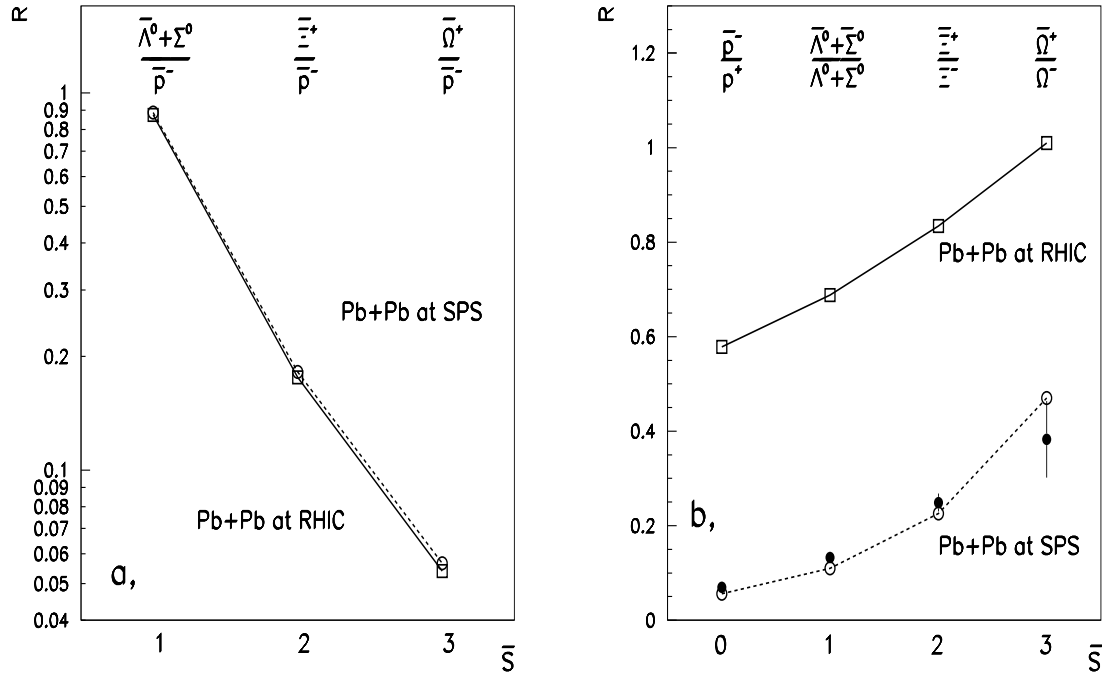


Figure 14. Particle ratios in Pb + Pb collisions calculated for SPS (open circle) and predicted for RHIC (open square). Experimental data (filled circle) are from Refs. [6,7]. In Fig. 14(a) the ratios for SPS and RHIC are practically the same.

Some particle ratios are shown for the SPS and RHIC energies in Fig. 14. For the RHIC calculations the same parameters were used as for the SPS, except the number of produced quark antiquark pairs ($N_{q\bar{q}} = 834, N_{s\bar{s}} = 92$ at SPS; $N_{q\bar{q}} = 4200, N_{s\bar{s}} = 462$ for RHIC). This number was determined by the requirement, that the same h^- multiplicity should be obtained as from HIJING.

REFERENCES

1. This note is a short summary of *The mischievous linear coalescence model and the correct quark counting in heavy ion collisions* by J. Zimányi, T. S. Biró and P. Lévai, (<http://sgi30.rmki.kfki.hu/~jzimanyi/coals.ps>).
2. T.S. Biró, P. Lévai, J. Zimányi, Phys. Lett. **B 347** (1995) 6.
3. T.S. Biró, P. Lévai, J. Zimányi, Phys. Rev. C 59 (1999) 1574
4. A. Bialas, Phys. Lett. B442 (1998) 449.
5. J. Zimányi, T.S. Biró, T. Csörgő, P. Lévai, hep-ph/9904501.
6. M. Kaneta et al., NA44 coll. J. Phys. **G: Nucl. Part. Phys.** 23 (1997) 1865
7. R. Caliendo et al., WA97 coll. J. Phys. **G: Nucl. Part. Phys.** 25 (1999) 171
8. C. Bormann for the NA49 Coll., J. Phys. **G: Nucl. Part. Phys.** 23 (1997) 1817.

2.2. J. Stachel: Fireball Model Predictions

Predictions for hadron yields in the central region at RHIC [1,2] can be based on a thermal model describing successfully the data obtained in present fixed target experiments at the AGS [3] and SPS [4,5] for central collisions of Si/S and Au/Pb beams with heavy targets (Au,Pb). The statistical model treats the system as a grand canonical ensemble and has two free parameters, a temperature T and a baryon chemical potential μ_B . Interactions of the particles are taken into account in form of an excluded volume correction corresponding to repulsion setting in for all hadrons at a radius of 0.3 fm [5]. The hadron yield ratios resulting from this model agree particularly well with the most complete set of data obtained sofar, the one for central Pb + Pb collisions at the SPS. Putting these results in perspective vis-a-vis the expected phase boundary between the quark-gluon-plasma and the hadron gas the hadrochemical freeze-out points are where one expects the phase boundary and it is suggestive that hadron yields are frozen at the point when hadronization is complete [6,7]. This suggests for RHIC a hadrochemical freeze-out temperature of about 170 MeV, the same as found at the SPS. The chemical potential is going to be small; here a value of 10 MeV is used as an upper limit. Strangeness and charge conservation require then values of μ_s and μ_{I_3} of 2.5 and -0.2 MeV.

The yield ratios as predicted for RHIC using these parameters are shown in Figure 15. The predictions are shown together with a best fit from the same model to data for central Pb + Pb collisions at the CERN SPS. One notices drastic differences as compared to present data, in particular in the yield ratios of antibaryons to baryons which are predicted at RHIC to be about 1 (see Fig. 15) due to the small chemical potential.

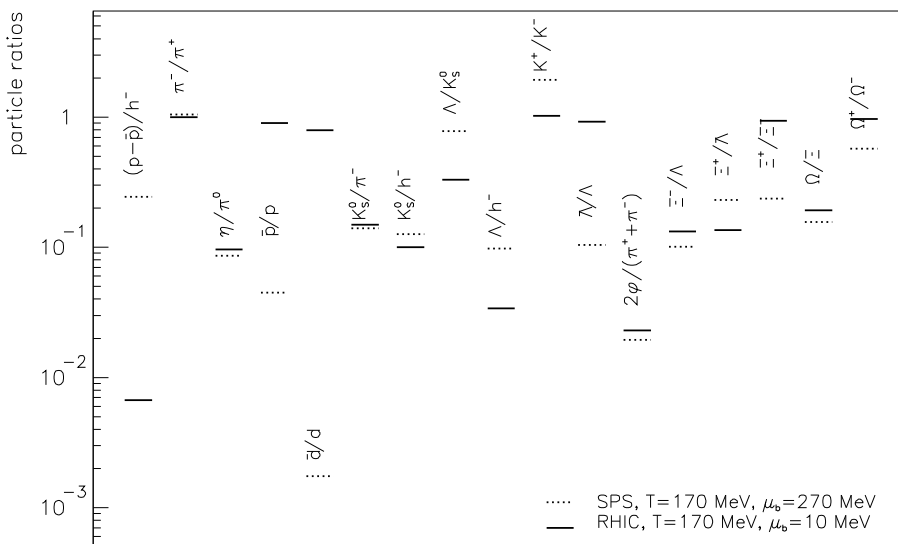


Figure 15. Hadron yield ratios from a thermal model (see text)

In order to predict absolute yields one has to estimate the volume per unit rapidity at the time when hadronization is complete. Starting from an initial temperature of $T_i = 500$ MeV at a time $\tau_i = 0.2$ fm/c and using a transverse expansion in the plasma of $\beta_{tp} = 0.16$ this volume is 3600 fm³ at a freeze-out temperature of 170 MeV. A selection of the predicted hadron yields are shown in Table 1. The model was used to compute yields for 193 different hadron species in total. The typical systematic error of this prediction, based

on the freeze-out parameters, is judged as follows. The chemical potential is bounded at a lower limit of 0. Yields for μ_b of 1 MeV were found to not be noticeably different. One finds small differences in the absolute yields of baryons with respect to antibaryons. The corresponding results are given in column 3 of Tab. 1 where they differ from the values for $\mu_B = 10$ MeV. Further, present SPS data put a lower limit of 160 MeV on the freeze-out temperature. Typical results for this lower temperature are given in column 4 of Tab. 1. Generally particle yields are reduced by about 10 % (as indicated for pions in Tab. 1), for the heaviest particles the reduction is 35 % (Ω , d).

Table 1
Hadron yields per unit of rapidity near mid-rapidity

particle	T=170 $\mu_b=10$	T=170 $\mu_b=1$	T=160 $\mu_b=10$
$\pi^- \approx \pi^+$	630		555
π^0	700		
η	68		
ρ^0	70		
ω	56		
η'	6		
ϕ	14		
$K^+ \approx K^- \approx K_s^0$	97		
p	62	59	
n	57		
\bar{p}	56	58	
$p - \bar{p}$	6	0.7	
Λ	32	30	
$\bar{\Lambda}$	29	30	
$\Lambda(1405)$	2		
$\Xi^- \approx \Xi^+$	4		3
$\Omega^- \approx \Omega^+$	0.78		0.50
d	0.23		0.14
\bar{d}	0.18		

REFERENCES

1. Work done in collaboration with P. Braun-Munzinger.
2. A complete version of the talk can be found at http://www.qm99.to.infn.it/rhic_pred/stachel/stachel.html
3. P. Braun-Munzinger, J. Stachel, J.P. Wessels, N. Xu, Phys. Lett. **B344** (1994) 43.
4. P. Braun-Munzinger, J. Stachel, J.P. Wessels, N. Xu, Phys. Lett. **B365** (1996) 1.
5. P. Braun-Munzinger, I. Heppe, and J. Stachel, preprint nucl-th/9903010.
6. P. Braun-Munzinger and J. Stachel, Nucl. Phys. **A606** (1996) 320.
7. J. Stachel, Proceedings Int. Nucl. Phys. Conference Paris, August 1998, Nucl. Phys. **A** (1999) in print.

2.3. J. Rafelski: Strange Hadrons from QGP at RHIC

(Strange) hadronic particle abundances and spectra have been obtained [1], assuming a thermally equilibrated, chemically non-equilibrated deconfined QGP source undergoing a sudden freeze-out at RHIC. The theoretical framework of this approach is presented in some detail in the contribution by **Jean Letessier** [2].

From the study of the SPS data we deduce the universality of physical properties of hadron chemical freeze-out [2,3], occurring practically at the same condition as the kinetic freeze-out. The differences in system dependent particle m_{\perp} -slopes are understood to be a consequence of differences in collective flow in a deconfined QGP source. We believe that this remains the general situation at the 10 times higher collision energies reached at RHIC. We expect that the QGP break-up temperature $T_f^{\text{SPS}} \simeq 145 \pm 5$ MeV will see a minor upward change to say $T_f^{\text{RHIC}} \simeq 150 \pm 5$ MeV. Thus all we need to do in order to characterize particle production at RHIC is to adapt the picture of sudden QGP hadronization we have developed to the greater longitudinal flow, lower baryon density environment we expect at RHIC.

In our understanding of the freeze-out, there is complete absence of a pure hadronic gas, or even a mixed phase in the dense matter evolution. The deconfined QGP state evaporates over a few fm/c in time, during which time it is kept by a balance of dynamical processes near to the freeze-out temperature: the evaporation and work done against the vacuum cool the surface down, which is internally heated by the explosive energy flows. Empirical evidence at SPS suggests that the transverse flow velocity imparted on emitted hadrons does not surpass $v_{\perp} \simeq c/\sqrt{3} \equiv v_{\text{sound}}$. The other QGP properties imparted on hadronic particles within this sudden freeze-out model are:

$$\begin{aligned} \lambda_s = 1 &\Leftrightarrow \langle s - \bar{s} \rangle = 0; \\ \gamma_q \simeq 1.5\text{--}1.8 &\Leftrightarrow \text{entropy enhancement in plasma and gluons converted to quarks;} \\ \gamma_s > 1 &\Leftrightarrow \text{strangeness equilibrates with } T > T_f^s > T_f; \\ \text{unknown : } \lambda_q &\Leftrightarrow \text{baryon density; baryon:energy stopping relation.} \end{aligned}$$

However, λ_q must be smaller than seen at SPS in S–S ($\simeq 1.4$) so the range $\lambda_q \simeq 1.2 \pm 0.15$ which we base our predictions on, is nearly certainly correct.

We thus expect to find, at RHIC, a kinetically equilibrated, but chemically evolving, QGP source, with direct hadron emission from a flowing surface, just as we found in the case of SPS energy collisions. We expect, based and compared to the Pb–Pb 158A GeV results:

- Shape identity of RHIC m_{\perp} and y spectra of antibaryons \bar{p} , $\bar{\Lambda}$, $\bar{\Xi}$, since in our approach there is no difference in their production mechanism;
- The m_{\perp} -slopes of these antibaryons should be very similar to the result we have from Pb–Pb 158A GeV since only a slight increase in the freeze-out temperature occurs, and no increase in collective transverse flow is expected;
- Major changes compared to SPS must be expected in rapidity spectra of mesons, baryons and antibaryons.

Work on an extension of our sudden hadronization model to include the expected substantial longitudinal flow at RHIC is underway. We report here preliminary results that deserve immediate attention. Strangeness is here an extremely interesting observable for:

Table 2

Sample of hadron ratios expected at RHIC, see text explanation of the model parameters

Ratios	RHIC-1)	RHIC-2)
Ξ/Λ	0.18 ± 0.02	0.14 ± 0.02
$\bar{\Xi}/\bar{\Lambda}$	0.25 ± 0.03	0.19 ± 0.03
$\bar{\Lambda}/\Lambda$	0.49 ± 0.15	0.49 ± 0.15
$\bar{\Xi}/\Xi$	0.68 ± 0.15	0.68 ± 0.15
Ω/Ξ	0.14 ± 0.03	0.10 ± 0.03
$\bar{\Omega}/\bar{\Xi}$	0.20 ± 0.03	0.15 ± 0.03
$\bar{\Omega}/\Omega$	1.	1.
$\frac{(\Omega+\bar{\Omega})}{(\Xi+\bar{\Xi})}$	0.17 ± 0.01	0.12 ± 0.01
$\frac{(\Xi+\bar{\Xi})}{(\Lambda+\bar{\Lambda})}$	0.21 ± 0.02	0.17 ± 0.02
K^+/K^-	1.35 ± 0.25	1.34 ± 0.25
p/\bar{p}	2.9 ± 1.5	2.9 ± 1.5
$\bar{\Lambda}/\bar{p}$	2.4 ± 0.3	1.8 ± 0.3
h^-/B	$4.6 -2+10$	$4.6 -2+10$

Table 3

RHIC rapidity distribution of all (anti)baryons assuming flat net-baryon rapidity distribution

dN/dy	Baryons	Antibaryons
protons	25 (p)	8.5 (\bar{p})
Λ	42 (Λ)	20 ($\bar{\Lambda}$)
Ξ	7.5 (Ξ)	5 ($\bar{\Xi}$)
Ω	1 (Ω)	1 ($\bar{\Omega}$)

1. Gluons make strangeness effectively in the early stage of the collision and thus at SPS strangeness is more central than baryon number. It is possible that this will be even more accentuated at RHIC leading to ‘strangeness dominance’ at central rapidity.

2. Central strangeness production will further be enhanced by an increase in initial temperature compared to SPS. We anticipate at RHIC stunning strange hadron abundance anomalies.

In Table 2 we present two scenarios which differ by the strangeness phase space occupancy excess: we take in both cases the chemical freeze-out temperature and velocity $T_f = 150 \text{ MeV}$, $v_{\perp} = 1/\sqrt{3} \simeq 0.58c$ and the chemical light quark conditions: $\lambda_q = 1.2 \pm 0.15$, $\gamma_q = 1.8$, as well as QGP strangeness conserving $\lambda_s = 1$, but, in first case, we take $\gamma_s = 2$ and in second $\gamma_s = 1.5$. To obtain the rapidity densities one of the key distributions needs to be known: we use a net baryon density $d(B - \bar{B})/dy \simeq 70$, which if nearly flat in $\Delta y \simeq \pm 3$, allows to fully account for all participating baryons in a zero impact parameter collision. Employing the ratios given as RHIC-1) in Table 2 we obtain the results shown in Table 3, which imply hyperon-dominance of the baryon yields. RHIC-2) scenario would further enhance the hyperon-dominance.

The key result we see in this extrapolation of the SPS results to RHIC is that the (anti)baryon abundances (rapidity distributions) are strongly strangeness dominated, which as we have been arguing in past two decades is the characteristic behavior in QGP phase break-up.

REFERENCES

1. J. Rafelski, <http://www.qm99.to.infn.it/program/qmprogram.html> .
2. J. Letessier, <http://www.qm99.to.infn.it/program/sessio3/sessio3.html>;
J. Letessier and J. Rafelski, in this volume, *Strange Particle Chemical Freeze-Out*.
3. J. Rafelski and J. Letessier, “Hadrons from Pb–Pb collisions at 158A GeV”, nucl-th/9903018; J. Letessier and J. Rafelski, *Phys. Rev.* **C59** (1999) 947; *Acta Phys. Pol.*, **B30** (1999) 153; *J. Phys.*, **G25** (1999) 295.

2.4. S.E. Vance: Baryons, Junctions and Hyperons

Recently, the baryon junction mechanism was proposed to explain the observed baryon stopping at the SPS[1,2]. The baryon junction appears when writing the QCD gauge invariant operator of the baryon, being the vertex which links the three color flux (Wilson) lines flowing from the valence quarks. Being a gluonic configuration, the junction can be easily transported into the mid-rapidity region in hadronic reactions. There near mid-rapidity, as the strings connecting the junction to the valence quarks fragment, a baryon is produced being composed of three sea quarks. This gluonic mechanism is also able to explain[3] a striking, preliminary measured baryon asymmetry observed approximately 8 units of rapidity away from the proton’s fragmentation region in ep collisions at HERA.

The valence baryon junction mechanism was recently extended and a new mechanism for anti-hyperon production was proposed[4]. Like the valence baryon junction mechanism, this junction-anti-junction loop ($J\bar{J}$) mechanism is also derived from the topological gluon structure of the baryon and originates in the context of Regge phenomenology. The ($J\bar{J}$) mechanism was shown to strongly enhance the anti-hyperon yields in nuclear collisions and is needed to provide reasonable anti-hyperon to hyperon ratios. Both of these mechanisms were implemented in HIJING/ $\bar{B}\bar{B}$, a modified version of the HIJING event generator.

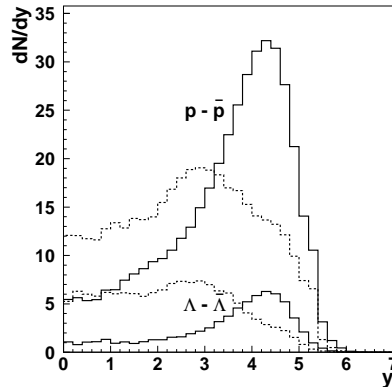


Figure 16. Predictions for the initial valence proton rapidity distribution (upper two curves) and for the initial valence hyperon rapidity distribution (lower two curves) are given for Au+Au collisions at $E_{cm} = 200$ AGeV by HIJING (solid) and HIJING/ $\bar{B}\bar{B}$ (dashed).

The effects of these mechanisms at RHIC energies were explored using HIJING/B \bar{B} . Estimates for the initial valence p and Λ rapidity distributions in $Au + Au$ collisions at RHIC energies ($\sqrt{s} = 200$ GeV) for $b = 0$ fm are shown in Figure 16. HIJING/B \bar{B} predicts approximately twice the initial number of valence protons and five times the initial number of valence hyperons of HIJING at mid-rapidity leading to a prediction of twice the initial baryon density, $\rho(\tau_0) \approx 2\rho_0 \approx 0.3/\text{fm}^3$. Estimates for the total \bar{p} and $\bar{\Lambda}$ have also been made (see Figure 17), where it was found that at these energies, the yields of the anti-baryons are only sensitive to the relative string fragmentation probability of producing diquarks to quarks, and not to the small cross section for producing $J\bar{J}$ loops. While the $J\bar{J}$ loops do not significantly effect the absolute yields, they are important in producing rapidity correlations between baryons and anti-baryons, such as the $\Delta^{++}(uuu)$ and $\bar{\Omega}^+(\bar{s}\bar{s}\bar{s})$, which are absent in present baryon pair production schemes.

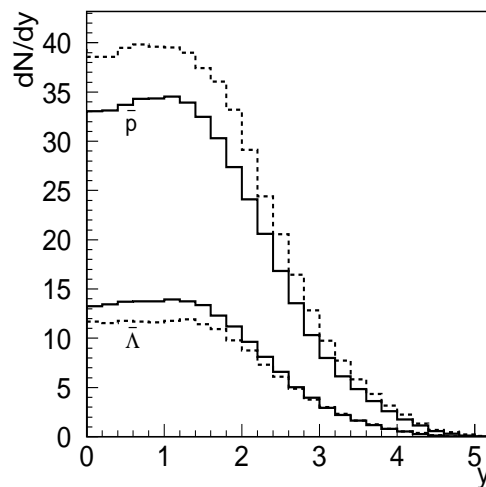


Figure 17. Predictions for the initial \bar{p} and $\bar{\Lambda}$ rapidity distributions are given for HIJING (solid lines) and for HIJING/B \bar{B} (dashed curves) for Au+Au collisions at $E_{cm} = 200$ AGeV for $b = 0$ fm.

In the phenomenology associated with the baryon junction, many new states being gauge invariant combinations of junctions, anti-junction, quark and anti-quarks[5] were predicted, e.g. a quarkless hybrid glueball ($J\bar{J} = M_0^J$). The experimental search for these states has been inconclusive (presumably due to their large decay widths), with only several broad resonances remaining as possible candidates. We propose that the effect of large glueball states (e.g. $S_0^6 = (J\bar{J}J\bar{J}J\bar{J})$) can be observed at RHIC by seeing a non-trivial rapidity correlation between two baryons (e.g. pp rapidity correlations) in NN collisions (see [6]).

REFERENCES

1. D. Kharzeev, Phys. Lett. **B378** (1996) 238, nucl-th/9602027.
2. S.E. Vance, M. Gyulassy and X.N. Wang, Phys. Lett. **B443** (1998) 45; nucl-th/9806008.

3. B. Kopeliovich and B. Povh, Phys. Lett. **B446** (1999) 321; hep-ph/9810530.
4. S.E. Vance and M. Gyulassy, Phys. Rev. Lett. in press, nucl-th/9901009.
5. G.C. Rossi, G. Veneziano, Nucl. Phys. **B123** (1977) 507; Phys. Rep. **63** (1980) 153.
6. http://www.qm99.to.infn.it/rhic_pred/vance/vance.html

3. HBT AND COLLECTIVE FLOW CORRELATIONS

3.1. S. Pratt: HBT at RHIC

Prediction of QGP time delay too late for these proceedings. [M.G.: Look for it at RHIC in spite of heretical views in sec. 3.3. See D.H. Rischke, M. Gyulassy, NPA 608 (1996) 479]

3.2. D. Teaney: Nutcracker Flow and HBT

Flow in non-central collisions at the SPS has been studied experimentally [3] and theoretically [4,5] and shows sensitivity to the EoS. However, high and low energy collisions have different acceleration histories, due to the QCD phase transition. In the mixed phase the EoS is soft [6]. For AGS/SPS collision energies the matter is produced close to the “softest point” and therefore the initial transverse acceleration is small. Using a bag model EoS and fixing the initial entropy to the SPS multiplicity, we have simulated PbPb collisions at $b=8\text{fm}$ with boost invariant hydrodynamics. The matter expands preferentially in the impact parameter direction (the x direction). Since the matter is produced close to the softest point, it retains its initial elliptic shape, accelerating only in the late hadronic stages. For higher collision energies, the hot QGP is formed well above the transition temperature and the early pressure forces early acceleration. Unfortunately, the final radial flow velocity at RHIC is quite similar to the SPS [7] as is the final elliptic flow [1,8]. The early quark push has important consequences, however. The resulting velocity has a long time, $\sim 10\text{fm}/c$, to change the matter distribution before freeze-out. The stiff QGP in the center, with $T \gg T_c$, pushes against the soft matter on the exterior, with $T \approx T_c$, producing two shell-like structures which separate in the x direction leaving two holes in the y direction. Since the final distorted distribution rather resembles a nut and its shell, we call this picturesque configuration the *nutshell*. In Fig.18(a) we show the “nutty” energy distribution in the transverse plane at zero rapidity. No shell like structures are seen for an ideal gas EoS. The matter expands elliptically and the final distribution resembles a gaussian.

The early acceleration may be seen with HBT interferometry since the early velocity increases the size of the system. From the two pion correlation function, the following radii may be extracted by carefully choosing the pion pair momenta [9,1].

$$R_{xx}^2 = \langle x^2 \rangle - \langle x \rangle^2 \tag{9}$$

$$R_{yy}^2 = \langle y^2 \rangle - \langle y \rangle^2 \tag{10}$$

(The average momentum of the pair was taken to be 500 MeV). These radii are shown in Fig.18(b) for PbPb collisions at $b=8\text{ fm}$, as a function of the pion multiplicity scaled by the number of participants to central collisions (not $b=8\text{ fm}$). R_{xx} and R_{yy} are shown for a bag model EoS and for a simple resonance gas EoS. For low energies near the left hand side of the plot, the two EoS show approximately the same radii, roughly corresponding

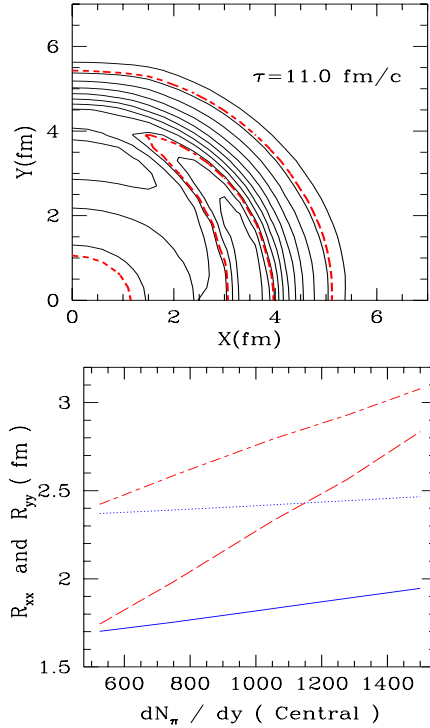


Figure 18. (a) Typical matter distribution in the transverse plane at mid rapidity, calculated using boost invariant hydrodynamics with a bag model EoS, for a PbPb collision at $b=8$ fm at RHIC ($dN_\pi/dy = 850$). The solid lines show contours of constant energy density. The inner and outer dashed lines show temperatures $T=140$ MeV and $T=120$ MeV respectively. (b) HBT radii, R_{xx} and R_{yy} , as a function of the final pion multiplicity. For a resonance gas EoS $p = .2\epsilon$, the solid lines and dotted lines show R_{xx} and R_{yy} respectively. For a bag model EoS, the dashed and dashed-dotted lines show R_{xx} and R_{yy} respectively.

to the initial elliptic shape of the matter distribution. For a simple resonance gas EoS the HBT Radii show little energy dependence, while for an EoS with the phase transition the Radii increase steadily with beam energy. The rapid increase of R_{xx} can be understood qualitatively. The nutshells separate at higher collision energies and leave a large homogeneous region in the center. The constancy of R_{xx} for an ideal gas EoS reflects the energy gradients in the final distribution. For an EoS with a phase transition, the source function is “box” like and the “box” increases in size, while for an ideal gas EoS the source function is more gaussian.

Other signatures of the nutcracker flow were presented in [1] and similar qualitative features were found by [8,10].

Acknowledgments: Work supported by U.S. DOE, under Contract No. DE-FG02-88ER4038.

REFERENCES

1. D. Teaney and E. Shuryak, nucl-th/9904006 (1999).
2. D. Teaney, E. Shuryak and H. Sorge:
http://www.qm99.to.infn.it/rhic_pred/teaney/teaney.html
3. H. Appelshäuser et al., (NA49 Collaboration), Phys. Rev. Lett. **80**, 4137(1998).
4. J.Y. Ollitrault, Phys. Rev. **D46**, 229(1992); Phys. Rev. **D48**, 1132(1993).
5. H. Sorge, Phys. Rev. Lett. **78**, 2309(1997); nucl-th/9812057 (1998).
6. C.M. Hung, E.V. Shuryak, Phys. Rev. Lett. **75**, 4003(1995).
7. S. Bass, A. Dumitru, et al. , nucl-th/9902062.
8. P. Kolb, et al. these proceedings
9. U. Heinz and B.V. Jacak, prepared for Ann. Rev. Nucl. Part. Sci, **49**(1999).
10. M. Gyulassy, et al. these proceedings.

3.3. B.R. Schlei: The QGP Stall or Not

In 1996, D.H. Rischke and M. Gyulassy [1] proposed to use the time-delay signal in Bose-Einstein correlations (BEC) as a signature for the possible formation of a quark-gluon plasma (QGP) in relativistic heavy-ion collisions. In particular, they suggested to measure the ratio of the transversal interferometry radii, R_{out}/R_{side} , which can be obtained by fitting experimental BEC data with a parametrization introduced by G. Bertsch [2] et al. in 1988. The transverse radius parameter R_{out} has compared to the transverse radius parameter R_{side} an additional temporal dependence which should be sensitive to a prolonged lifetime of a fireball, in case a QGP was formed in a relativistic heavy-ion collision. This latter phenomenon is known under the term “QGP stall”. In the following, I shall explain why I believe that the time-delay signal in Bose-Einstein correlations *is not* a good signature for the possible formation of a QGP.

Let us consider two quite different equations of state (EOS) of nuclear matter within a *true* relativistic hydrodynamic framework (i.e., HYLANDER-C) [3]. The first one, EOS-I, has a phase-transition to a QGP at $T_C = 200 \text{ MeV}$ ($\epsilon_C = 1.35 \text{ GeV}/fm^3$) [4]. The second EOS, EOS-II, is a purely hadronic EOS, which has been extracted from the transport code RQMD (cf., Ref. [5]) under the assumption of fully achieved thermalization. If one assumes for each EOS *different* initial conditions before the hydrodynamical expansions, one can fit simultaneously hadronic single inclusive momentum spectra and BEC, which have been measured recently by the CERN/NA44 and CERN/NA49 Collaborations (cf., [4,5]), respectively. In particular, for the acceptance of the NA44 experiment a ratio $R_{out}/R_{side} \approx 1.15$ was found [4] while using both EOS, EOS-I and EOS-II. Little difference was seen in the BEC of identical pion pairs while considering the two different EOS.

In the following, we shall assume for central Au+Au collisions at BNL/RHIC beam energies a set of fireball initial conditions, IC-I, which are similar to those as described in Ref. [7]. From these fireball initial conditions, IC-I, single inclusive momentum spectra have been calculated while using EOS-I and EOS-II in the hydrodynamic expansions. We note, that the rapidity spectra of both calculations differ in width and normalization significantly [6]. Fig. 19. shows, that the isotherms of the transversely expanding fluids at longitudinal coordinate $z = 0$ also differ significantly. Since there will be only one set of measured data, we shall fit the calculation using EOS-II to the single inclusive momentum spectra of the calculation using EOS-I. In doing so, we find new initial conditions, IC-II

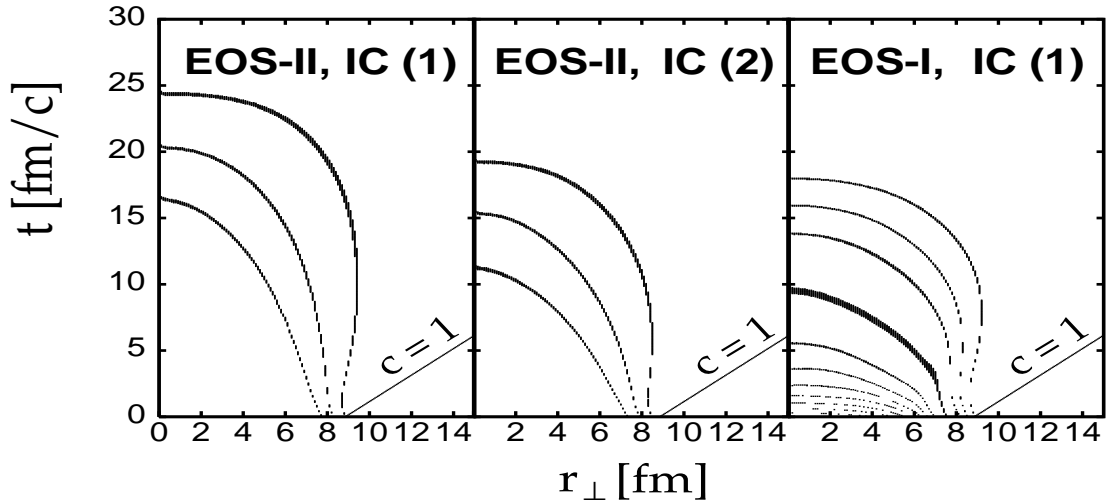


Figure 19. Isotherms in steps of $\Delta T = 20 \text{ MeV}$. The outer contours equal $T_f = 140 \text{ MeV}$.

[6]. But now the space-time picture of the evolving fireball at freeze-out is again very similar to the one using EOS-I with IC-I.

If one calculates BEC of identical pion pairs or identical kaon pairs, respectively, one finds [6] while comparing the calculations using EOS-I with IC-I and EOS-II with IC-II, respectively, *no* significant differences in the extracted ratios R_{out}/R_{side} regardless of the pair kinematics under consideration. In particular, the assumption of the PHENIX detector acceptance [6] leads to a ratio $R_{out}/R_{side} \approx 1.65$ for both choices of EOS.

In summary, the larger ratio R_{out}/R_{side} at RHIC beam energies appears to be rather a consequence of the expected higher energy deposit in the fireball during the heavy-ion collision, but it appears *not* to be an indicator of the present or absent phase-transition to a QGP. Of course, more theoretical analysis is necessary, but there is strong evidence, that BEC do not provide a good QGP signature, since we do not understand the initial state of a heavy-ion collision well enough yet.

REFERENCES

1. D.H. Rischke, M. Gyulassy, Nucl. Phys. A608 (1996) 479.
2. G. Bertsch, M. Gong, M. Tohyama, Phys. Rev. C37 (1988) 1896.
3. B.R. Schlei, Heavy Ion Phys. 5 (1997) 403.
4. B.R. Schlei, et al., to appear in Eur. Phys. J. C (1999).
5. B.R. Schlei, D. Strottman, N. Xu, Phys. Rev. Lett. 80 (1998) 3467, and Refs. therein.
6. Check the web-site <http://www.nis.lanl.gov/~bschlei/qm99.html>
7. B.R. Schlei, D. Strottman, Phys. Rev. C59 (1999) R9.

3.4. J.Y. Ollitrault: Elliptic Flow

See J.Y. Ollitrault, Phys. Rev. D46, 229 (1992).

3.5. D. Molnar: Elliptic Flow via Inelastic Parton Cascade

Transverse energy and elliptic flow are of recent theoretical interest because they signal collectivity and thus may be sensitive to a possible phase transition. Also, they are relatively easy to measure and therefore will be one of the first results at RHIC.

Until thermal and chemical equilibrium are shown to be achieved in relativistic heavy ion collisions, a transport theory approach is absolutely necessary. Two forerunners [1,2] of the present study utilize the ZPC elastic parton cascade [5], which has colorless gluons with a single elastic $2 \rightarrow 2$ process. However, for the question of chemical equilibration it is essential to include inelastic processes, too.

If we insist on having on-shell partons, the simplest set of particle number changing processes consists of a $2 \rightarrow 3$ and a $3 \rightarrow 2$ process. By adding these two new processes to ZPC, we developed an on-shell inelastic parton cascade, MPC [3].

To have a well-defined theoretical model that is independent of the code, we regard MPC as a tool for solving the Boltzmann transport equation

$$\begin{aligned}
p^\mu \partial_\mu f_1 &= 2 \int_2 \int_3 \int_4 \left[\frac{(2\pi)^6}{g^2} f_3 f_4 - \frac{(2\pi)^6}{g^2} f_1 f_2 \right] W_{12 \rightarrow 34} \delta(12 - 34) \\
&+ 3 \int_2 \int_3 \int_4 \int_5 \left[\frac{(2\pi)^6}{g^2} f_4 f_5 - \frac{(2\pi)^9}{g^3} f_1 f_2 f_3 \right] W_{123 \rightarrow 45} \delta(123 - 45) \\
&+ 2 \int_2 \int_3 \int_4 \int_5 \left[\frac{(2\pi)^9}{g^3} f_3 f_4 f_5 - \frac{(2\pi)^6}{g^2} f_1 f_2 \right] W_{12 \rightarrow 345} \delta(12 - 345), \quad (11)
\end{aligned}$$

where f is the Lorentz invariant phase space density, the Lorentz invariant W -s are proportional to the corresponding $2 \rightarrow 2$, $2 \rightarrow 3$ and $3 \rightarrow 2$ matrix elements, $f_i \equiv f(p_i, x)$, $f_i \equiv \int \frac{d^3 p_i}{E(p_i)}$, and g is the degeneracy of the partons. Furthermore, combinations like $12 - 34$ are for $p_1 + p_2 - p_3 - p_4$, etc., and the arguments of $W_{12 \rightarrow 34}(p_1, p_2, p_3, p_4)$, etc., are suppressed.

For simplicity, we took our gluons to be massless. The $2 \rightarrow 2$ and $2 \leftrightarrow 3$ differential cross sections were taken to be uniform in phase space with theta function cutoffs $\Theta((p_i + p_j)^2 - \mu^2)$ for each possible pair of ingoing and each possible pair of outgoing particles in order to prevent collinear collisions. The leftover momentum dependence of the cross sections was fixed by imposing energy independent *total* crosssections for $\mu^2 = 0$, while the $3 \rightarrow 2$ cross section was given by detailed balance. The gluon degeneracy was $g = 16$ (3 colors).

Fig. 20. shows the transverse energy loss in a one-dimensional Bjorken expansion starting from a locally thermal distribution. Keeping the total $2 \rightarrow X$ cross section constant, we studied how the energy loss changes with the ratio of the elastic and inelastic part of the cross section. We considered three cases: fully elastic, 50% inelastic, and fully inelastic. The initial conditions were the same as in Ref. [1]: $\tau_0 = 0.1 \text{fm}/c$, $T_0 = 500 \text{MeV}$, $dN/d\eta = 400$, $-5 \leq \eta \leq 5$, $A_t = 100 \text{fm}^2$, and we averaged over 20 events.

We can see that the transverse energy at midrapidity is sensitive only to the total $2 \rightarrow X$ cross section. With increasing inelasticity there is somewhat less work done because opening up the inelastic channels leads to parton production which compensates for the decrease of work. There also shows a tendency that until the cross section is

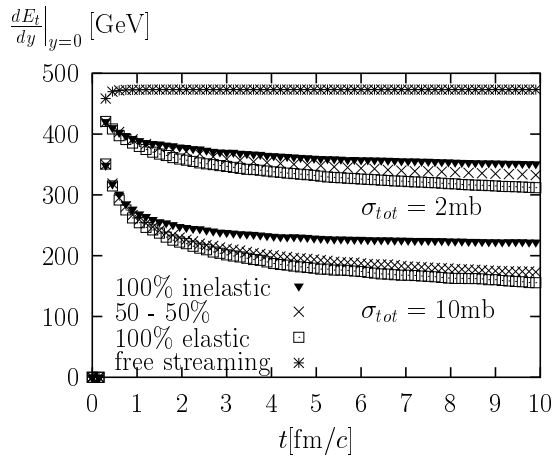


Figure 20. E_t evolution for a 1-dimensional Bjorken expansion

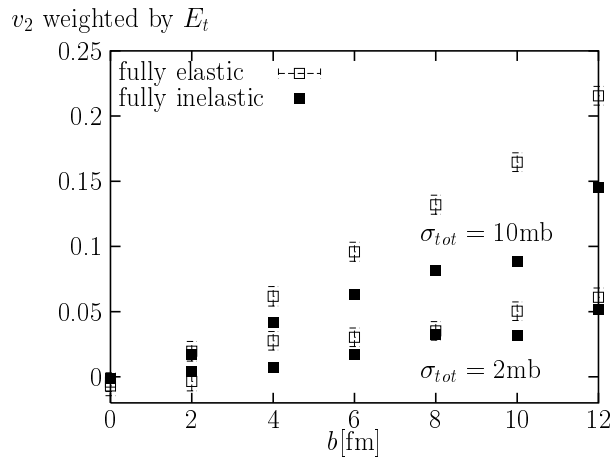


Figure 21. Elliptic flow vs. centrality and inelasticity

dominantly inelastic the energy loss is rather insensitive to the degree of inelasticity.

Fig. 21. shows how the elliptic flow parameter v_2 changes with centrality and inelasticity. We took a similar initial condition as Ref. [2] but with $dN/d\eta d^2x_t = 3/\text{fm}^2$, $T_0 = 500\text{MeV}$, $R = 7\text{fm}$, $-5 \leq \eta \leq 5$. We averaged over 20 events.

As we go from the fully elastic to the fully inelastic case elliptic flow drops, showing that the details of the microscopic dynamics *are* important. This is also supported by another study [6] using the RQMD 3.0 event generator.

The 50% reduction of v_2 is *in addition* to the original 50% drop relative to ideal hydrodynamics [4] given by dissipative corrections at the elastic level [2]. The centrality dependence is very similar to that from hydrodynamics.

A study with more realistic gluon cross sections and diffuse initial geometry is underway.

REFERENCES

1. M. Gyulassy, Y. Pang and B. Zhang, Nucl. Phys. **A626**, 999 (1997); and references therein
2. B. Zhang, M. Gyulassy and C.M. Ko, nucl-th/9902016; and references therein
3. D. Molnar, Quark Matter '99 transparencies at http://nt3.phys.columbia.edu/people/molnard/QM99_transparencies/
4. J.-Y. Ollitrault, Phys. Rev. **D46**, 229 (1992)
5. B. Zhang, Comput. Phys. Commun. **109**, 193 (1998)
6. H. Sorge, Phys. Rev. Lett. **82**, 2048 (1999)

4. JETS AND PENETRATING PROBES AT RHIC

4.1. R. Rapp: Low Mass Dileptons

Low-mass dilepton spectra in (ultra-) relativistic heavy-ion collisions are expected to provide information on the in-medium properties of the light vector mesons in connection with signals from chiral symmetry restoration. At RHIC energies, the major experimental challenge is a large (combinatorial) background which limits the sensitivity to well-defined resonance structures. In this contribution [1] we will thus address the question to what extent ρ and ω spectral functions are affected in meson-dominated matter (following paragraph) and how this reflects itself in space-time integrated dilepton spectra to be measured at RHIC (last paragraph).

Thermal dilepton radiation from a hot and dense medium is governed by the thermal expectation value of the electromagnetic current-current correlator, Π_{em} . Up to invariant masses of ~ 1 GeV its hadronic part can be accurately saturated with light vector mesons (Vector Dominance Model). The pertinent thermal dilepton production rate can then be expressed through the vector meson spectral functions, $\text{Im}D_V$, as

$$\frac{dN_{ll}}{d^4x d^4q} = -\frac{\alpha^2}{\pi^3} \frac{f^B(q_0; T)}{M^2} \text{Im}\Pi_{em}(q; T) \quad , \quad \text{Im}\Pi_{em}(q; T) = \sum_{V=\rho,\omega,\phi} \frac{m_V^4}{g_V^2} \text{Im}D_V(q; T) \quad , \quad (12)$$

where f^B denotes a thermal Bose distribution function and M is the invariant mass of the lepton pair. Medium effects in the ρ propagator are accounted for through modifications in the $\rho \rightarrow \pi\pi$ width (most notably from a Bose enhancement of the two-pion states characterizing 'stimulated emission') and by collisions with surrounding thermal π , K and ρ mesons via s -channel resonance formation (ω , a_1 , K_1 , f_1 , etc.), see, *e.g.*, Refs. [3]. At a temperature $T=150$ MeV the total thermal broadening of $\text{Im}D_\rho$ amounts to about 80 MeV with no significant shift in mass, cf. left panel of Fig. 22.

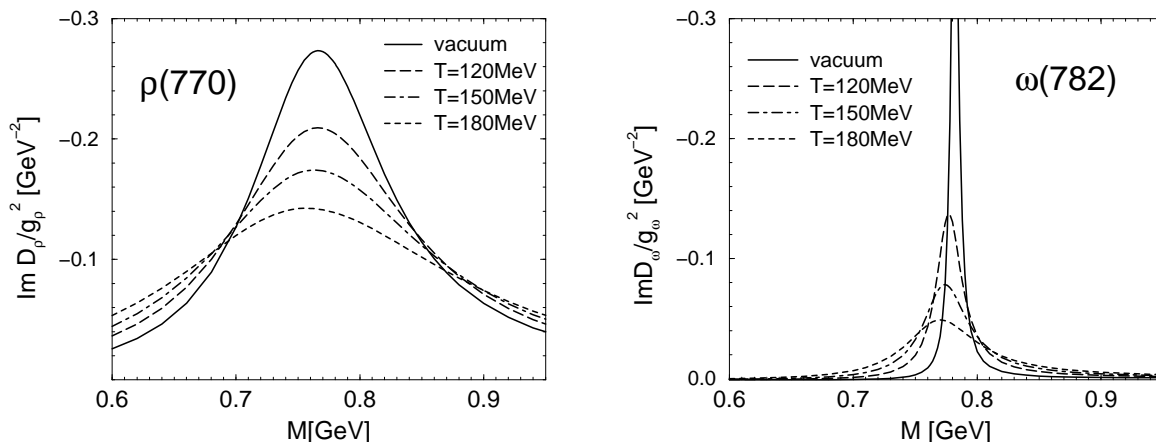


Figure 22. ρ - (left panel) and ω - (right panel) spectral functions (weighted by the corresponding VDM coupling constant) at fixed 3-momentum in a thermal meson gas.

Along similar lines, the ω meson decay width (which in free space consists of a combination of $\rho\pi$ and direct 3π decays) has been evaluated including both pion- and rho Bose factors as well as the in-medium ρ spectral function. Also, an in-medium selfenergy from $\pi\omega$ scattering through the $b_1(1235)$ resonance [4] has been inferred from the 70% branching ratio of the free $b_1 \rightarrow \omega\pi$ decay. As a result, the finite temperature ω spectral function exhibits a broadening of several times its vacuum width, cf. right panel of Fig. 22.

Dilepton spectra from ρ and ω decays are readily calculated by integrating the thermal rate, Eq. (12), over the hadronic space-time volume of a central Au+Au collision at RHIC. For that we assumed an adiabatic expansion (including a mixed phase at $T_c=180$ MeV) with an entropy over baryon density of $s/n_B = 220$ together with a charged particle multiplicity of $dN_{ch}/dy \simeq 1100$ around midrapidity. The 3-volume expansion has been modelled in accordance with hydrodynamic simulations. The final 3-momentum integrated dilepton invariant mass spectra from $\rho, \omega \rightarrow e^+e^-$ decays are displayed in Fig. 23. The broad ρ structure can most likely not be disentangled from the large background ex-

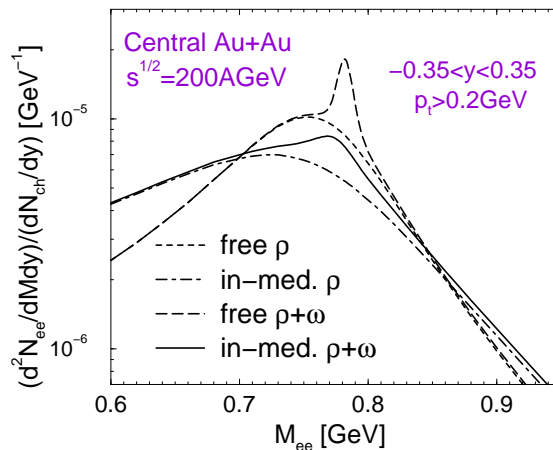


Figure 23. Dilepton spectra from a thermal fireball through $\rho, \omega \rightarrow e^+e^-$ decays in the hadronic phase including a schematic acceptance for the PHENIX detector.

pected in PHENIX. On the other hand, the thermal broadening of the ω (leading to a net ~ 40 MeV wide signal) may be 'just right', *i.e.*, narrow enough to be possibly detectable above the background and the ρ contribution, but substantially wider than the free ω , which allows for a discrimination from (free) ω decays after freeze-out and thus enables important insights into its finite temperature behavior.

REFERENCES

1. For the transparencies, see: <http://www.qm99.to.infn.it/program/qmprogram.html>.
2. See the PHENIX homepage at <http://www.phenix.bnl.gov/>.
3. R. Rapp and C. Gale, Phys. Rev. **C**, in print, hep-ph/9902268 and references therein.
4. E.V. Shuryak, Nucl. Phys. **A533** (1991) 761; K. Haglin, Nucl. Phys. **A584** (1995) 719; C. Gale, D. Seibert and J. Kapusta, Phys. Rev. **D56** (1997) 508.

4.2. I. Vitev: Jet Quenching in Thin Plasmas

One of the predicted new observables in nuclear collisions at RHIC energies ($\sqrt{s} \sim 200$ AGeV) is jet quenching due to gluon bremsstrahlung. We study the detailed gluon probability distribution in the case of few ($n_s = 1, 2, 3$) scattering centers which leads to the suppression of the high p_\perp tails of the hadronic spectra [1,2].

The Landau-Pomeranchuk-Migdal (LPM) effect [3], first studied for the case of QED, plays an important role in the non-abelian gauge theories as well, leading to nontrivial results [4]. Unlike in electrodynamics, where the energy of the final electron and photon can be directly measured, the energy of a single parton is not measurable. Therefore, in order to test the non-abelian energy loss of jets [4], the detailed form of the angular distribution, $dN_g/dy d^2\vec{k}_\perp$, of induced gluon radiation must be known. The angular integrated energy loss, dE/dx , is theoretically interesting but insufficient to address the experimentally accessible question of how much are moderate $p_\perp \sim 3 - 10$ GeV pions expected to be suppressed relative to their known spectrum in elementary nucleon-nucleon reactions.

We use the Gyulassy-Wang (GW) model of locally thermally equilibrated plasma [4]. In the case of one scattering center there are three relevant diagrams [2] that give the gluon conditional probability distribution:

$$\begin{aligned} \frac{dN_g^{(1)}}{dy d^2\vec{k}_\perp} &= C_R \frac{\alpha_s}{\pi^2} \left(\vec{H}^2 + R(\vec{B}_1^2 + \rho(\vec{b}_1) \vec{C}_1^2) - R(\vec{H} \cdot \vec{B}_1 \cos(t_{10}\omega_0)) \right. \\ &\quad \left. - R\rho(\vec{b}_1/2) (\vec{H} \cdot \vec{C}_1 \cos(t_{10}\omega_{10}) - 2\vec{C}_1 \cdot \vec{B}_1 \cos(t_{10}\omega_1)) \right), \end{aligned} \quad (13)$$

where we have rearranged the terms following [5] and introduced the following notation:

$$\begin{aligned} \vec{H} &= \frac{\vec{k}_\perp}{k_\perp^2}, \quad \vec{C}_1 = \frac{(\vec{k} - \vec{q}_1)_\perp}{(k - q_1)_\perp^2}, \quad \vec{B}_1 = \vec{H} - \vec{C}_1; \\ \omega_0 &\equiv k_\perp^2/2\omega = 1/t_f, \quad \omega_1 \equiv (k - q_1)_\perp^2/2\omega, \quad \omega_{10} \equiv \omega_1 - \omega_0. \end{aligned} \quad (14)$$

The phase factors $\omega_0, \omega_1, \omega_{10}$ have the formation physics built in. The normalized transverse density profile $\rho(\vec{b}_1) \equiv T(\vec{b}_1)/T(0)$ eliminates rescatterings of the emitted gluon at large angles and keeps consistency with the geometry of the process. $R \equiv C_A/C_R$ is 1 or 9/4 for gluon or quark jets respectively.

Similar formulas can be derived for the case of two and three scattering centers [1]. In all cases a couple of simple analytical limits can be obtained.

$$\lim_{k_\perp \rightarrow 0} \frac{dN_g^{(n_s)}}{dy d^2\vec{k}_\perp} = \frac{dN_g^{(0)}}{dy d^2\vec{k}_\perp}, \quad \lim_{k_\perp \rightarrow \infty} \frac{dN_g^{(n_s)}}{dy d^2\vec{k}_\perp} = \frac{dN_g^{(0)}}{dy d^2\vec{k}_\perp} (1 + R)^{n_s}. \quad (15)$$

Therefore we can make an ansatz, allowing us to consider multiple scattering extrapolations:

$$\Delta \frac{dN_g^{(n_s)}}{dy d^2\vec{k}_\perp} \approx \frac{dN_g^{(0)}}{dy d^2\vec{k}_\perp} \left((1 + R)^{n_s} - 1 \right) f \left(\frac{\lambda\mu^2}{\omega}, \frac{k_\perp^2}{\mu^2} \right). \quad (16)$$

From Fig.24. one can see that the quantitative agreement between the scaled result for one scattering center and the exact and much more complicated $n_s = 2$ result is within 5% everywhere in the kinematically allowed domain.

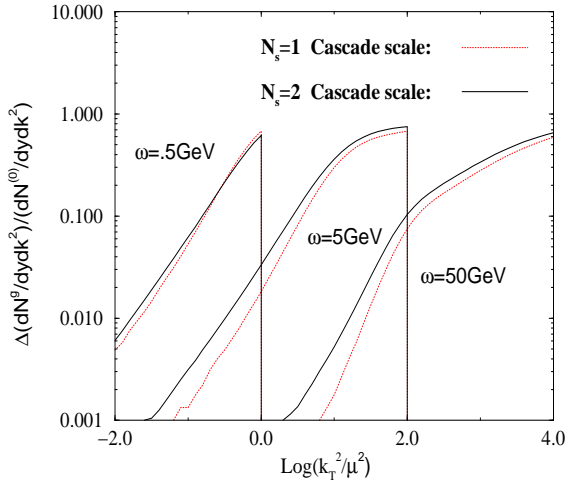


Figure 24. Scaling of the gluon probability distribution with the number of scattering centers. $E_{jet} = 50 \text{ GeV}$

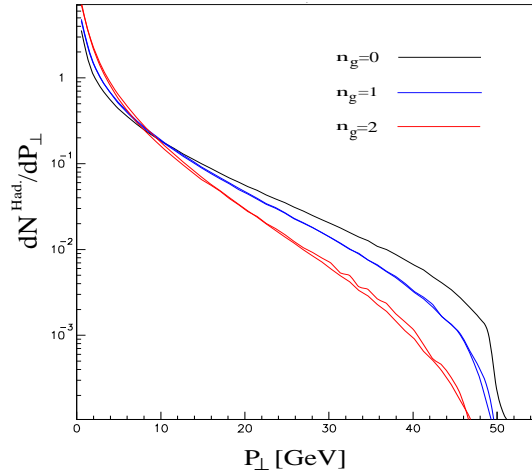


Figure 25. High p_{\perp} tail suppression of the hadronic distribution for partonic event $E_{C.M.} = 20 \text{ GeV}$ (JETSET).

Jet quenching occurs even in free space where there are no final state interactions, leading to characteristic double-logarithmic probability distribution [1,5]. In practice, the large logarithm implies that multiple gluon emission must also be considered. This leads to a Sudakov form factor for the jet and a probabilistic Alterelli-Parisi parton shower [7].

The final state multigluon shower can be calculated most readily by one of the many Monte-Carlo event generators [6] that encode empirical parton to hadron fragmentation functions and thus allow the detailed study of the effect of parton showering on the final hadron distributions. We have used the Lund JETSET [6] string fragmentation routine to hadronize a high energy partonic event accompanied by gluon bremsstrahlung. Fig.25. clearly shows the quenching effect of the medium induced and modified radiation.

Considering the significant role that “hard” physics will play at RHIC energies as compared to SPS we expect this effect to be roughly on the order of two.

REFERENCES

1. M. Gyulassy, P. Levai, I. Vitev, hep-ph/9907461 and see in this proceedings.
2. I. Vitev, <http://www.qm99.to.infn.it/program/qmprogram.html>
3. L. D. Landau and I. J. Pomeranchuk, Dokl. Akad. Nauk. USSR **92**, 92(1953); A. B. Migdal, Phys. Rev. **103**, 1811 (1956).
4. M. H. Thoma and M. Gyulassy, Nucl. Phys. B **351**, 491 (1991); M. Gyulassy and X.-N. Wang, Nucl. Phys. B **420**, 583 (1994); A.H.Mueller, S. Peigné, D. Schiff, Nucl. Phys. B **483** (1997) 291;
5. J. F. Gunion and G. Bertsch, Phys. Rev. D **25**, 746 (1982).
6. X.-N. Wang and M. Gyulassy, Phys. Rev. D **44** (1991) 3501; X.-N. Wang, Comp. Phys. Comm. **83** (1994) 307; T. Sjöstrand, Comp. Phys. Commun. **27**, 243 (1982); B. Andersson, G. Gustafson, G. Ingelman, and T. Sjöstrand, Phys. Rep. **97**, 31 (1983);
7. R. D. Field, *Applications of perturbative QCD*, Addison-Wesley, 1989.

4.3. A.M. Snigirev: Monojet Rate at RHIC

Hard jet production is considered to be an effective probe for formation of super-dense matter – quark-gluon plasma (QGP) in future heavy ion collider experiments at RHIC and LHC. High p_T parton pair (dijet) from a single hard scattering is produced at the initial stage of the collision process (typically, at ~ 0.01 fm/c). It then propagates through the QGP formed due to mini-jet production at larger time scales (~ 0.1 fm/c), and interacts strongly with the comoving constituents in the medium. The various aspects of hard parton passage through the dense matter are discussed intensively [1–12]. In particular, the strong acoplanarity of dijet transverse momentum [1–3], the dijet quenching (a suppression of high p_T jet pairs) [5] and a monojet-to-dijet ratio enhancement [8] were originally proposed as possible signals of dense matter formation in ultrarelativistic ion collisions.

In the simple QCD picture for a single hard parton-parton scattering without initial state gluon radiation (i.e. when jets from dijet pair escape from primary hard scattering vertex back-to-back in azimuthal plane with equal absolute transverse momentum values, $p_{T1} = p_{T2}$) a monojet is created only if one of the two hard partonic jets loses so much energy due to multiple scattering in the dense matter that effectively we can detect only one single jet in the final state. The monojet rate is obtained by integrating the dijet rate over the transverse momentum p_{T2} of the second (unobserved) jet with the condition that p_{T2} be smaller than the threshold value p_{cut} (or the threshold jet energy $E_T = p_{cut}$ ¹). Then rate of dijets R^{dijet} with $p_{T1}, p_{T2} > p_{cut}$ and monojets R^{mono} with $p_{T1} > p_{cut}$ ($p_{T2} < p_{cut}$) in central AA collisions is calculated as integral over all possible jet transverse momenta p_{T1}, p_{T2} and longitudinal rapidities y_1, y_2 .

At first in the framework of the simple model [14] we demonstrate that monojet-to-dijet ratio can be related to mean the acoplanarity measured in the units of the jet threshold energy, namely

$$\frac{R^{mono}}{R^{dijet}} \propto \frac{\langle |K_T| \rangle}{E_T}. \quad (17)$$

The results of physics simulation have been obtained in the three scenarios for jet quenching due to collisional energy losses of jet partons in mid-rapidity region $y = 0$ [11, 14]: (i) no jet quenching, (ii) jet quenching in a perfect longitudinally expanding QGP (the average collisional energy losses of a hard gluon $\langle \Delta E_g \rangle \simeq 10$ GeV, $\langle \Delta E_q \rangle = 4/9 \cdot \langle \Delta E_g \rangle$), (iii) jet quenching in a maximally viscous quark-gluon fluid, resulting in $\langle \Delta E_g \rangle \simeq 20$ GeV. Initial state gluon radiation has been taken into account with the PYTHIA Monte-Carlo model [15] at c.m.s. energy $\sqrt{s} = 5.5A$ TeV.

Thus we conclude that rescattering of hard partons in medium results in weaker E_T -dependence of ratio R^{mono}/R^{dijet} to $\langle |K_T| \rangle / E_T$. With growth of energy losses the ratio we are interested in has a tendency to be constant, what would be interpreted as the signal of super-dense matter formation.

REFERENCES

¹Due to fluctuations of the transverse energy flux arising from a huge multiplicity of secondary particles in the event, the "true" jet recognition in ultrarelativistic heavy ion collisions is possible beginning only from some energy threshold [13].

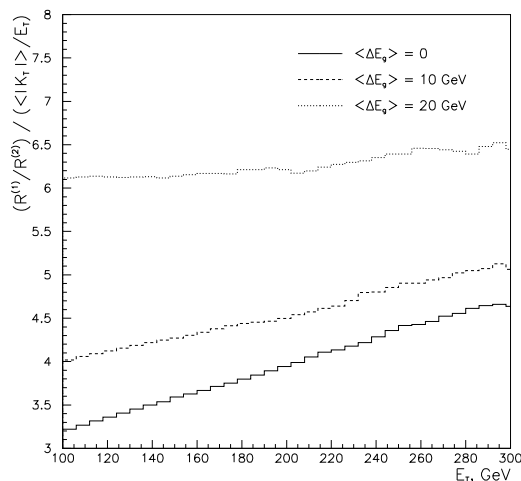


Figure 26. (Monojet/dijet)/(mean acoplanarity/ E_T) ratio as a function of jet energy threshold E_T .

1. D.A.Appel, Phys. Rev. D33 (1986) 717
2. J.P.Blaizot, L.D.McLerran, Phys. Rev. D34 (1986) 2739
3. M.R.Rammerstorfer, U.Heinz, Phys. Rev. D41 (1990) 306
4. M.G.Ryskin, Sov. J. Nucl. Phys. 52 (1990) 139
5. M.Gyulassy, M.Plumer, Phys. Lett. B 234 (1990) 432
6. M.H.Thoma, Phys. Lett. B 273 (1991) 128
7. M.Gyulassy, X.-N.Wang, Nucl. Phys. B420 (1994) 583; X.-N.Wang, M.Gyulassy, M.Plumer, Phys. Rev. D51 (1995) 3436
8. M.Plumer, M.Gyulassy, X.-N.,Wang, Nucl. Phys. A590 (1995) 511
9. R.Baier, Yu. L.Dokshitzer, S.Peigne, D.Schiff, Phys. Lett B 345 (1995) 277; R.Baier, Yu. L.Dokshitzer, A.H.Mueller, S.Peigne, D.Schiff, Nucl. Phys. B 483 (1997) 291; 484 (1997) 265; R.Baier, Yu. L.Dokshitzer, A.H.Mueller, D.Schiff, Nucl. Phys. B 531 (1998) 403; Phys. Rev. C58 (1998) 1706
10. B.G.Zakharov, JETP Lett. 65 (1997) 615
11. I.P.Lokhtin, A.M.Snigirev, Phys. At. Nucl. 60 (1997) 360; Z.Phys C73 (1997) 315
12. I.P.Lokhtin, A.M.Snigirev, Phys. Lett. B 440 (1998) 163
13. N.A.Kruglov, I.P.Lokhtin, L.I.Sarycheva, A.M.Snigirev, Z. Phys. C 76 (1997) 99
14. I.P.Lokhtin, L.I.Sarycheva, A.M.Snigirev, Phys. Atom. Nucl. 62 (1999), in press
15. T.Sjostrand, Comp. Phys. Com. 82 (1994) 74

4.4. D.K. Srivastava: Direct Photons and Dileptons at RHIC

The radiation of single photons from quark matter has recently been estimated to the order of two loops [1]. This provides a large bremsstrahlung contribution as well as a new mechanism of quark-annihilation with scattering. Together these lead to a much large radiation of photons than the estimates based on one-loop calculations [2]. These rates along with the radiations from the hadronic matter due to the hadronic reactions have been used to estimate the yield of photons from $Pb + Pb$ collisions at RHIC [3] with the assumption that a thermally and chemically equilibrated quark gluon plasma is formed at $\tau_0 = 0.5$ fm/c and having $T_0 = 310$ MeV, corresponding to $dN_\pi/dy = 1734$ (see Fig. 27).

However, it is rather unlikely that the QGP would be created in a chemically equilibrated form. The radiation of photons from an equilibrating plasma [4] due to Compton and annihilation processes (alone) and also from the pre-equilibrium stage (i.e., pre-thermally equilibrated quark matter) within a parton cascade model [5] are given in Fig. 28.

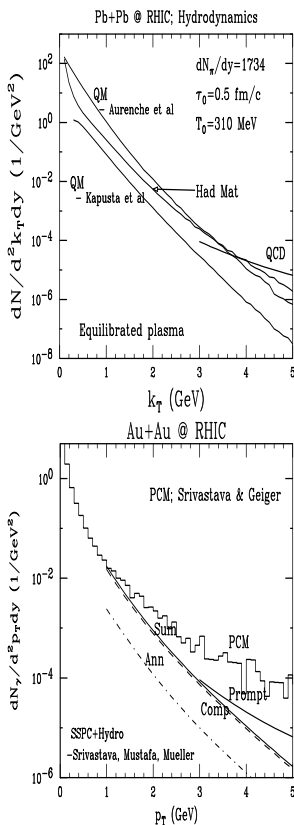


Figure 27. Radiation of photons from central collision of lead nuclei at RHIC energies from the hadronic matter (in the mixed phase and the hadronic phase) and the quark matter (in the QGP phase and the mixed phase). The contribution of the quark matter while using the rates obtained by Kapusta et al. and Aurenche et al. and those from hard QCD processes are shown separately.

Figure 28. Radiation of photons from central collision of gold nuclei at RHIC energies from an equilibrating plasma where the initial conditions are taken from a self-screened parton cascade model. Only Compton and annihilation processes are included. The pre-equilibrium contribution within a parton cascade model is also shown.

Correlated charm decay presents the largest source of dileptons at RHIC energies, though the spectrum of such dileptons will depend sensitively on the extent of thermalization of the charm quarks and D-mesons [6]. In case it is absent the upper limit of dilepton production can be seen in Fig. 29, while the radiation of dileptons due to annihilation of quarks (alone) from a chemically equilibrating plasma [4] is shown in Fig. 30.

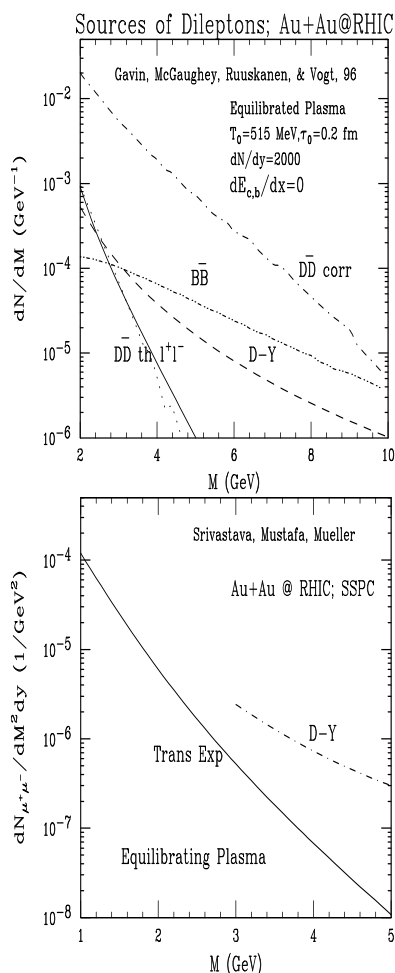


Figure 29. Sources of high mass dileptons. A thermalized and chemically equilibrated QGP is assumed. The correlated charm and bottom decay is estimated assuming no energy-loss for the heavy quarks and no thermalization of D mesons.

Figure 30. Radiation of large mass dileptons from a chemically equilibrating quark gluon plasma.

REFERENCES

1. P. Aurenche, F. Gelis, H. Zaraket, and R. Kobes, Phys. Rev. D 58 (1998) 085003.
2. J. Kapusta, P. Lichard, and D. Seibert, Phys. Rev. D 44 (1991) 2774; Erratum, ibid D 47 (1993) 4171.
3. D. K. Srivastava, nucl-th/9904010, and to appear in Euro. Phys. Journ. C.
4. D. K. Srivastava, M. G. Mustafa, and B. Müller, Phys. Rev. C 56 (1997) 1064.
5. D. K. Srivastava and K. Geiger, Phys. Rev. C 58 (1998) 1734.
6. S. Gavin, P. L. McGaughey, P. V. Ruuskanen, and R. Vogt, Phys. Rev. C 54 (1996) 2606.

4.5. Z. Lin: Open Charm and Drell Yan at RHIC

One of the signatures for the formation of the quark-gluon plasma in heavy ion collisions at RHIC is the thermal dileptons emitted from such a matter. However, dileptons from both final heavy meson decays and initial Drell-Yan processes can contribute significantly to the continuum background, thus making it difficult to observe the thermal dileptons from the quark-gluon plasma. Quantitative studies of dilepton production from these processes are therefore essential.

Although production of charm quarks in proton-proton interactions can be reason-

ably well described by perturbative QCD, their fragmentation to charm mesons is non-perturbative. In order to calculate the final open charm observables, one needs to know the intrinsic transverse momentum k_t of the partons inside a proton, the K-factor which takes into account higher order contributions, and the parameter ϵ when the Peterson charm fragmentation function is used. From the fit to E791 data on the angular distribution between the charm and anti-charm mesons, k_t is found to be about 1 GeV. In fitting the charm meson p_\perp spectra from E706 and the p_\perp^2 spectra from E769, $K_c \simeq 3$ and $\epsilon \simeq 0.01$ are obtained. For Drell-Yan processes, we simply take the leading-order (LO) $q\bar{q}$ annihilation cross sections with a K-factor, $K_{DY} = 1.7$, determined by fitting to E772 data. Thermal dileptons from the LO $q\bar{q}$ annihilation from the quark-gluon plasma is calculated in the parton cascade model ZPC, where the initial gluon and quark distributions are taken from the HIJING model.

In Fig. 31, we show the dilepton invariant-mass spectra for central Au+Au collisions at RHIC. The solid, dashed and dot-dashed curves represent dileptons from correlated open charm decays, Drell-Yan processes, and LO thermal $q\bar{q}$ annihilation, respectively. The dilepton yield from open charm decays is lower than earlier estimates where the charm fragmentation function is taken to be $\delta(1-z)$, which is equivalent to taking $\epsilon = 0$ in the Peterson formula. For dileptons with mass below 10 GeV, the open charm contribution is higher than that from Drell-Yan processes, which is much larger than the thermal dilepton yield from LO $q\bar{q}$ annihilation from the quark-gluon plasma.

Our preliminary results thus indicate that to detect the thermal dileptons from the quark-gluon plasma does not seem feasible. However, we have underestimated the thermal dilepton yield. First, only $2 \rightarrow 2$ partonic processes are included in ZPC, so the total number of partons does not increase as the system evolves. Secondly, we have not included thermal dilepton production from gluonic processes such as $gq \rightarrow q\gamma^*$ and $gg \rightarrow q\bar{q}\gamma^*$. Although cross sections for these two processes are suppressed by α_s and α_s^2 , respectively, they could have large effects on the thermal dilepton yield because gluons greatly outnumber quarks in the early partonic stage of heavy ion collisions at RHIC.

Also, results on open charms are only based on information taken from pp collisions. In heavy ion collisions, charm mesons are expected to undergo final-state hadronic interactions. We have recently studied the hadronic scatterings between charm mesons and hadrons such as pion, rho, and nucleon and have found that the charm meson spectra are significantly affected by these rescatterings. The increase of the invariant mass of charm meson pairs due to scatterings in hadronic matter leads to an increase of the invariant mass of dileptons from their decays, and this has been shown to provide a possible explanation for the observed large dimuon enhancement in the intermediate-mass-region (IMR) of 1.5 – 2.5 GeV in the NA50 experiment at SPS. Such final-state hadronic rescattering effects are different from those due to initial-state interactions, e.g., an increase of the parton intrinsic k_t in the nuclei effectively boosts the charm pair in the transverse direction, thus causing negligible change of the pair mass spectra and the resulting IMR dileptons from their decays.

At RHIC energies and beyond, partonic interactions of charm quarks in the quark-gluon plasma are also possible, such as the energy loss of fast quarks. Even a moderate energy loss of 0.5 GeV/fm has been found to suppress by an order of magnitude both the yield of high p_\perp charm mesons and that of large invariant-mass dileptons from their decays.

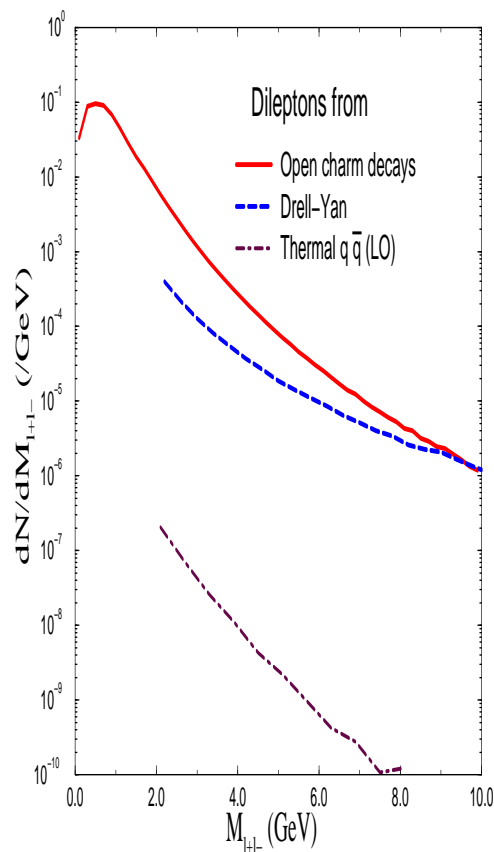


Figure 31. Dilepton spectra from central Au+Au collisions at RHIC.

For a more reliable evaluation of the dilepton spectra in heavy ion collisions at RHIC, one needs to further study the effects due to final-state interactions of both charm quarks and charm mesons as well as thermal dilepton production from gluonic processes in the quark-gluon plasma.

REFERENCES

1. S. Gavin, P.L. McGaughey, P.V. Ruuskanen and R. Vogt, Phys. Rev. C, 54 (1996) 2606; E. Shuryak, Phys. Rev. C, 55 (1997) 961; Z. Lin, R. Vogt and X.-N. Wang, Phys. Rev. C, 57 (1998) 899; B. Zhang, M. Gyulassy and Y. Pang, Phys. Rev. C, 58 (1998) 1175; Z. Lin, C. M. Ko and B. Zhang, preprint nucl-th/9905003.
2. See transparencies at either <http://www.qm99.to.infn.it/program/qmprogram.html> or <http://nt3.phys.columbia.edu/people/zlin/ZLIN/publication.html>.
3. This work was supported in part by NSF Grant PHY-9870038, Welch Foundation Grant A-1358, and Texas Advanced Research Project FY97-010366-068.

4.6. R. Thews: B_c Mesons at RHIC

The B_c meson is the bound state of $b\bar{c}$ (or $\bar{b}c$) whose recent detection is the first step toward completion of the spectroscopy of heavy quark mesonic states. The b - c states have properties that conveniently fill the gap between the J/ψ and the Υ states. Thus it is probable that at RHIC the B_c mesons will serve as a probe of deconfined matter [1]. We find that significant differences arise for B_c formation in deconfined and confined matter [2]. Our initial calculations suggest that:

(a) The rates of normal hadronic production mechanisms at RHIC energies are not sufficient to produce a detectable number of B_c mesons.

(b) If a region of deconfined quarks and gluons is formed, the production (and survival) rate can be enhanced by several orders of magnitude.

(c) The observation of B_c mesons at RHIC would signal a source of deconfined charmed quarks, and the rate of B_c production will be a measure of the initial density and temperature of that source.

We note that the study of the b - c sector has the advantage of a long history of potential model analysis in the $b\bar{b}$ and $c\bar{c}$ sectors. These studies have provided robust predictions for the mass and lifetime of the B_c states [3], and the recent measurements by CDF are consistent with those calculations [4].

First, we estimate the production rate of B_c which one would expect if it results just from a superposition of the initial nucleon-nucleon collisions at RHIC. For heavy quark production, pQCD calculations for p - p interactions fit present accelerator data and bracket the RHIC energy range. Hard Probes Collaboration estimates indicate about 10 $c\bar{c}$ pairs and 0.05 $b\bar{b}$ pairs per central collision [5]. J/ψ and Υ production involves the use of some model, such as the Hard Probes color singlet fits [5], which predict bound state fractions of order somewhat less than the one percent level. A similar analysis for B_c production involves substantially smaller bound state fractions, since the b and \bar{c} must be produced in the same hard interaction, a process of order α_s^4 . At RHIC energies, typical values are $3 - 10 \times 10^{-5}$ [6], with the uncertainty from the scale choice in the pQCD calculations.

To get predictions for RHIC, we have looked at two scenarios for the luminosity. a) The “first year” case assumes a luminosity of $20 \mu b^{-1}$ with no trigger. b) The “design” luminosity assumes 65 Hz event rate with a 10% centrality trigger in Phenix, and uses 10^7 sec/year. The event rate predictions listed in the Table include both the weak branching fraction of the B_c plus the dimuon decay fraction for J/ψ . Results are also shown for J/ψ and Υ production and detection via $\mu^+\mu^-$ and the underlying heavy quark production which may be useful to make contact with other estimates. One sees easily that in this scenario there is no hope of seeing B_c ’s at RHIC.

Now the principal reason for this work - could deconfinement change the B_c production rate at RHIC? We have investigated the following scenario: For those events in which a $b\bar{b}$ pair are produced, the small B_c formation fraction could be avoided if one utilized the 10 $c\bar{c}$ pairs already produced by independent nucleon-nucleon collisions in the same event. This can occur if and only if there is a region of deconfinement which allows a spatial overlap of the b and c quarks. Also, one would expect additional $c\bar{c}$ production in the deconfined phase during its lifetime, as a result of the approach to chemical equilibration. The large binding energy of B_c (840 Mev) would favor their early “freezing out” and they will tend to survive as the temperature drops to the phase transition value. The same

effect for the B mesons and indeed for the B_s will not be so competitive, since these states are not bound at the initial high temperatures (or equivalently they are ionized at a relatively high rate by thermal gluons).

To do a quantitative estimate, we first utilized the quarkonium break-up cross section based on the operator product expansion [7], to calculate the dissociation rate of bound states due to thermal gluon collisions. We then used detailed balance for the formation rates, and calculated the equilibrium fraction of B_c/b -quarks (see Ref.[2] for details). At $T = 160$ GeV, this fraction drops to as low as a few percent, but it is at least a factor of 100 above the no-deconfinement scenario. To get a more realistic limit, we repeated the calculation, using only the initially-produced c quarks. This actually produces a much larger bound state fraction, since the c quark density only decreases with a T^3 volume factor rather than the $\exp(-m_c/T)$ of chemical equilibrium. The last three rows in the Table show the corresponding B_c numbers at RHIC in this scenario. They depend quite strongly on the initial temperature, which determines the final charm density through the assumed isentropic expansion.

We are in the process of refining these preliminary numbers. The kinetic equations will be followed numerically, using exact time evolution of the deconfined region and the effect of approach to chemical equilibrium for the charm quarks. It appears that the sensitivity to the parameters of the deconfined state will remain, making the observation of any B_c 's at RHIC both a "smoking gun" signal of deconfinement and a probe of the initial temperature of the system and the initial density of deconfined charm.

Observable	First Year	Design Luminosity
$c\bar{c}$ -pairs	$2.8 \cdot 10^8$	$6.5 \cdot 10^9$
$b\bar{b}$ -pairs	$1.2 \cdot 10^6$	$3.2 \cdot 10^7$
$J/\Psi \rightarrow \mu^+\mu^-$	$1.6 \cdot 10^5$	$3.9 \cdot 10^6$
$\Upsilon(1s) \rightarrow \mu^+\mu^-$	140	3800
$B_c \xrightarrow{2.5\%} J/\psi l\nu \xrightarrow{6\%} \mu^+\mu^-l\nu$		
(No Deconfined Phase)	0.05–0.18	1.5–4.9
(QGP+ $c\bar{c}$ in Chemical Equil.)	18	490
(Only initial $c\bar{c}$ at $T_o = 500$ MeV)	130	3530
(Only initial $c\bar{c}$ at $T_o = 400$ MeV)	235	6420
(Only initial $c\bar{c}$ at $T_o = 300$ MeV)	475	12900

REFERENCES

1. This work was initiated in collaboration with Jan Rafelski (Arizona) and Lewis Fulcher (Bowling Green), hep-ph/9905210; R. Seto, Ed., World Scientific, (Singapore 1999).
2. See transparencies at <http://www.physics.arizona.edu/~thews/bcmesons/qm99.html>.
3. L. Fulcher, hep-ph/9806444, sub. to *Phys. Rev. D*.
4. F. Abe *et al.*, CDF collaboration, *Phys. Rev. Lett.* **88**, 2432 (1988), and *Phys. Rev. D***58**, 2004 (1988).
5. "Hard Processes in Hadronic Interactions", *Int. J. Mod. Phys. A***10**, 2881 (1995).
6. K. Kolodziej and R. Ruckl, *Nucl. Instrum. Methods A***408**, 33 (1998).
7. D. Kharzeev and H. Satz, *Nucl. Phys. A***590**, 515c (1995).

4.7. R. Vogt: Predictions for J/ψ Suppression

The predictions are based on the model for J/ψ absorption by nucleons, comovers, and quark-gluon plasma discussed in the recent review [1]. As in Ref. [1], we take a nucleon absorption of 4.8 mb for color octet $c\bar{c}$ pairs and assume that the final-state charmonia can be broken up by mesonic comovers with an 0.67 mb cross section. The comover density is assumed to be proportional to the participant density in Au+Au collisions, n_{AuAu} .

The scale of the suppression is set by the transverse energy distribution of lepton pairs, shown in Fig. 32. In this calculation, the average transverse energy at a given impact parameter is the sum of hard and soft components and is approximately proportional to the number of collisions. Nuclear shadowing is included in the estimate of the hard component, see Ref. [2] for details. The distribution is plotted as a function of $E_T/E_{T,\text{max}}$ to be detector independent. Note that $E_{T,\text{max}} \sim 1600$ GeV for STAR and 700 GeV for PHENIX with an uncertainty of 10-20% depending on the shadowing model.

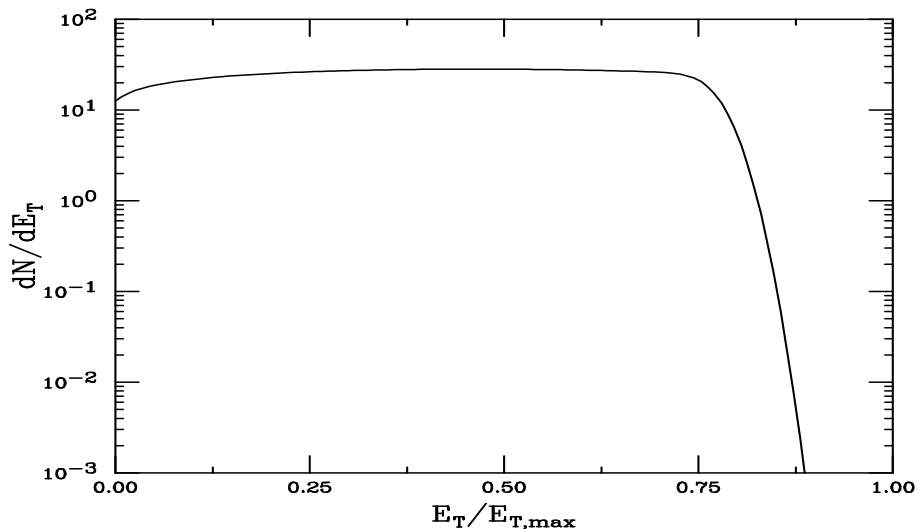


Figure 32. Lepton pair E_T distribution for RHIC.

The resulting J/ψ survival probabilities are shown in Fig. 33. Figure 33(a) is a completely hadronic scenario where the comover density is proportional to: n_{AuAu} , as for NA38 S+U; $2n_{\text{AuAu}}$, as for NA50 Pb+Pb; and $5n_{\text{AuAu}}$, beyond reasonable expectations for hadronic matter. In Fig. 33(b), plasma production is assumed in addition to comover absorption with density n_{AuAu} . Plasmas with 2 and 4 quark flavors are studied. The energy density as a function of E_T is determined from the hard and soft components to the average E_T [2]. When $n_f = 4$, only the χ_c and ψ' are suppressed, but for $n_f = 2$, direct J/ψ suppression occurs when $E_T/E_{T,\text{max}} \sim 0.2$. Note that plasma is created in even the lowest E_T 's produced at RHIC so that χ_c and ψ' suppression begin immediately in both cases.

The J/ψ and Drell-Yan cross sections were calculated in perturbative QCD with and without nuclear shadowing. In the lepton pair mass range $4 < m < 9$ GeV, $B\sigma_{J/\psi}/\sigma_{\text{DY}} \approx$

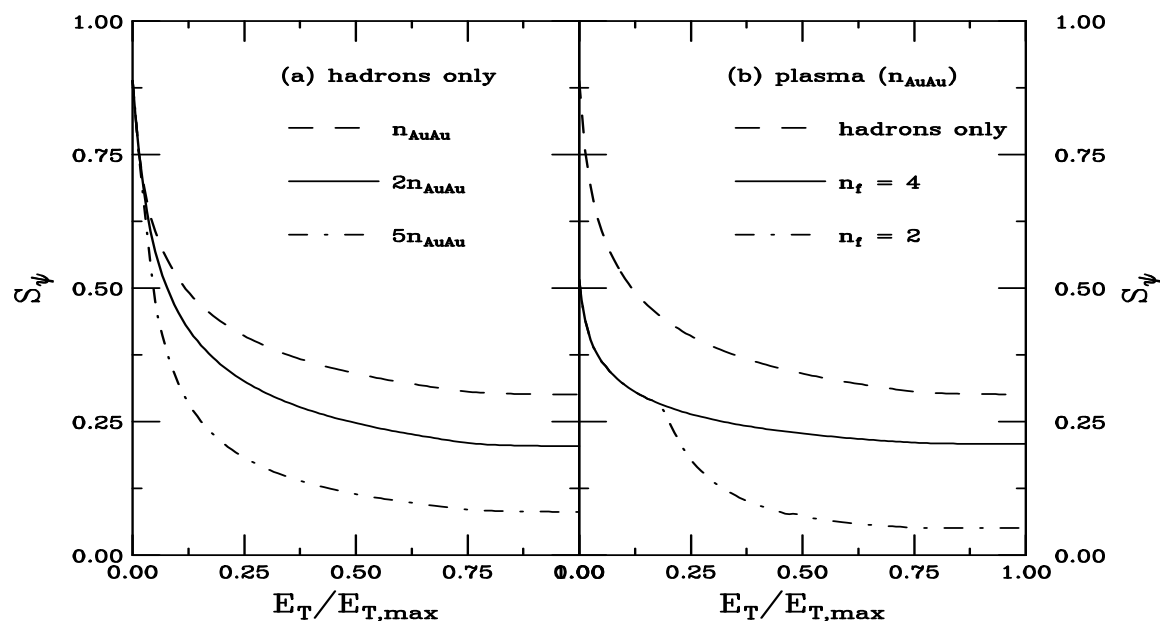


Figure 33. (a) J/ψ suppression by hadrons only for comover densities proportional to n_{AuAu} (dashed), $2n_{AuAu}$ (solid), and $5n_{AuAu}$ (dot dashed). (b) J/ψ suppression when quark-gluon plasma is produced for a plasma with 2 (dot dashed) and 4 (solid) quark flavors. The dashed curve is the same as in (a).

190 – 280 depending on the shadowing parameterization. The Drell-Yan cross section is calculated at next-to-leading order. The J/ψ cross section has been calculated both in the color evaporation model and in the non-relativistic QCD approach. The two methods yield nearly identical results at RHIC when no nuclear shadowing is included. See Ref. [2] for details of the cross section calculations and [3] for more numbers.

REFERENCES

1. R. Vogt, Phys. Rept. **310** (1999) 197.
2. V. Emel'yanov, A. Khodinov, S.R. Klein, and R. Vogt, LBNL-42900, to be submitted to Phys. Rev. **C**.
3. See <http://www.qm99.to.infn.it/program/qmprogram.html> for the entire talk.

5. EXOTIC POSSIBILITIES AT RHIC

5.1. J. Schaffner: $U_A(1)$ Restoration Signatures

Strange Signals from the Chiral Phase Transition? [1]

Recently, there have been strong indications from lattice calculations, that the chiral $U_A(1)$ symmetry is partially restored just above the critical temperature [2]. It was found that the screening mass splitting between the δ meson (the a_0 , a scalar-isovector meson) and the pion is reduced to about 5% or less. That means that the mass gap has changed by at least an order of magnitude. We are now going to discuss possible signals for RHIC associated with that effect. We explore the consequences with an $SU(3) \times SU(3)$ chiral Lagrangian. If the chiral $SU(3)$ symmetry is effectively restored, then the masses of the pion and the sigma meson and the masses of the eta and the δ meson are the same separately. If the chiral $U_A(1)$ symmetry is effectively restored, then this mass gap vanishes and all four meson masses are the same: $m_\pi = m_\sigma \approx m_\delta = m_\eta$ for $c \approx 0$ which gives two new observable effects for RHIC [3].

Prediction 1: the number of η s is enhanced by up to a factor four. The $a_0(980)$ meson has a width of $\Gamma = 50 - 100$ MeV. Its mass decreases with temperature, as seen on the lattice. Already below T_c the decay $a_0 \rightarrow \eta + \pi$ must be blocked by phase space (see figure). Also the matrix elements $\mathcal{M}(a_0 \rightarrow \eta_{ns} + \pi) = 4\lambda\sigma \approx 0$ in the chiral $SU(3)$ phase and $\mathcal{M}(a_0 \rightarrow \eta_s + \pi) = 2c \approx 0$ in the chiral $U_A(1)$ phase. Hence, the inelastic channels are closed. The elastic channels are still large as they are proportional to the coupling constant λ only. The a_0 can not decay to two pions which is forbidden by isospin. Also the decay to two kaons is heavily suppressed as the a_0 is actually lighter than one kaon alone. If the expansion from the chiral phase at T_c until the freeze-out temperature is fast enough (faster than the lifetime of the a_0 which is about 2–4 fm), then the numbers of a_0^{+-0} is three times the numbers of the pions due to isospin counting. As the a_0 decays mainly to η s and pions, the numbers of the η s can be increased by a factor up to four.

Prediction 2: The scalar κ (K_0^*) appears in the $K\pi$ mass spectrum. Recent studies of the πK scattering data show the existence of a broad scalar, strange resonance, the $\kappa(900)$ [4]. The mass of this particle couples also to the $U_A(1)$ anomaly, i.e. the mass splitting to the kaon is proportional to $\Delta m_K \propto c \cdot \sigma$. The matrix element for the strong decay of the κ to a pion and a kaon decreases in the chiral $U_A(1)$ phase from values around $\Gamma \approx .8$ GeV to $\Gamma \leq .2$ GeV. Hence, the barely visible broad resonance gets a much smaller width in the chiral $U_A(1)$ phase. As the mass of the κ approaches that of the kaon, the strong decay $\kappa \rightarrow K + \pi$ is blocked by phase space already below T_c . Now, if the system freezes out around T_c , there appears a cusp structure in the $K\pi$ invariant mass spectrum between $m_K = m_\pi = .64$ GeV and $m_\kappa = .9$ GeV due to the opening of the decay channel of the κ . The cusp should be pronounced as the width of the κ has substantially decreased.

Prediction 3: strange clusters of two baryons are formed at RHIC. The status quo about the baryon-baryon interaction is, that there is some (very limited) knowledge about the $N\Lambda$ ($N\Sigma$, $N\Xi$, $\Lambda\Lambda$) interactions from Λ (Σ , Ξ , $\Lambda\Lambda$) hypernuclei and $N\Lambda$, $N\Sigma$ scattering and Σ^- atoms. There is absolutely no experimental information about the $\Lambda\Sigma$, $\Lambda\Xi$, $\Sigma\Sigma$, $\Sigma\Xi$, $\Xi\Xi$ interaction at all. As hyperons are produced abundantly in relativistic heavy-ion collisions, this opens a new domain of strong interaction physics for RHIC. General $SU(3)$

flavor symmetry predicts that there are (quasi) bound states in e.g. Σ^+p , $\Sigma^-\Sigma^-$, $\Sigma^-\Xi^-$. The new Nijmegen soft-core potential fitted to scattering data indeed predicts bound states of $\Sigma\Sigma$, $\Sigma\Xi$, and $\Xi\Xi$ [5]. These exotica are detectable by their weak two-body (nonmesonic) decay to final states like proton, Λ , and Ξ^- . Detectable candidates are e.g. $(\Sigma^+p)_b \rightarrow p + p$, $(\Xi^0p)_b \rightarrow \Lambda + p$, $(\Xi^0\Lambda)_b \rightarrow \Xi^- + p$ or $\Lambda + \Lambda$, and $(\Xi^-\Xi^0)_b \rightarrow \Lambda + \Xi^-$. The branching ratio is about (5 – 30)% depending on the channel and the binding energy [6]. The decay length is about $c\tau = 1 - 5$ cm, the more bound the candidate, the shorter the lifetime. The production rates have been estimated to be around 0.02 to 0.001 per single event using RQMD2.4 and wavefunction coalescence [6].

REFERENCES

1. See http://www.qm99.to.infn.it/rhic_pred/schaffner/schaffner.html.
2. P. Chen et al., (1998), hep-lat/9812011.
3. J. Schaffner-Bielich, manuscript in preparation.
4. S. Ishida et al., Prog. Theor. Phys. 98 (1997) 621.
5. V.G.J. Stoks and T.A. Rijken, Phys. Rev. C (1999) (in press), nucl-th/9901028.
6. J. Schaffner-Bielich and R. Mattiello, manuscript in preparation.

5.2. D.H. Rischke: Parity Violation and Color Superconductors

We give a pedagogical discussion of how, for massless quarks at very high densities, the formation of a spin-zero color superconducting condensate spontaneously breaks both the axial $U(1)$ symmetry and parity [1]. This observation is implicit in the seminal work of Bailin and Love, is noted by Alford, Rajagopal, and Wilczek, and is explicitly discussed by Evans, Hsu, and Schwetz [2].

For simplicity, consider two degenerate flavors of quarks, and assume that a quark-quark condensate forms in the color-antitriplet channel [1–4]. For massless quarks, two of the four possible condensates with total spin $J = 0$ are [1]

$$\langle \phi_1^a \rangle = \epsilon^{abc} \epsilon_{fg} \langle q_f^{bT} C \gamma_5 q_g^c \rangle \quad \text{and} \quad \langle \phi_2^a \rangle = \epsilon^{abc} \epsilon_{fg} \langle q_f^{bT} C \mathbf{1} q_g^c \rangle, \quad (18)$$

where $a, b, c = 1, 2, 3$ are $SU(3)_c$ color indices, $f, g = 1, 2$ are $SU(2)_f$ flavor indices, and C is the charge conjugation matrix. $\phi_{1,2}^a$ are antitriplets under $SU(3)_c$ gauge transformations and singlets under $SU(2)_f$ rotations [1]. The condensate ϕ_1^a is even under parity, $J^P = 0^+$, while ϕ_2^a is odd, $J^P = 0^-$. There are two other condensates [1], but they do not change our qualitative arguments about parity violation, and so we omit them.

In the limit where mass and instanton-induced terms can be neglected, the effective Lagrangian for color superconductivity is

$$\mathcal{L}_0 = |\partial_\mu \phi_1|^2 + |\partial_\mu \phi_2|^2 + \lambda \left(|\phi_1|^2 + |\phi_2|^2 - |v|^2 \right)^2, \quad (19)$$

where $|\phi|^2 \equiv \sum_a (\phi^a)^* \phi^a$. When mass and instanton effects are neglected, the Lagrangian is symmetric under axial $U(1)$ transformations, which rotate ϕ_1^a and ϕ_2^a into each other.

Therefore, there is only one quartic coupling, λ . The Lagrangian (19) generates nonzero vacuum expectation values for the ϕ^a 's, which can be written as

$$\langle \phi_1^a \rangle = v^a \cos \theta \quad , \quad \langle \phi_2^a \rangle = v^a \sin \theta \quad . \quad (20)$$

Condensation picks out a given direction in color space for v^a , and a given value for θ . $v^a \neq 0$ breaks the $SU(3)_c$ color symmetry, which produces color superconductivity. $\theta \neq 0$ breaks the axial $U(1)$ symmetry. Further, whenever $\theta \neq 0$, there is a nonzero $J^P = 0^-$ condensate $\langle \phi_2^a \rangle$; this represents the spontaneous breaking of parity (relative to the external vacuum).

This breaking of parity is actually familiar from the spontaneous breaking of chiral symmetry. Consider two flavors of *massless* quarks; the effective potential is $O(4)$ -symmetric, involving the $J^P = 0^+$ σ - and $J^P = 0^-$ π -meson fields. For massless quarks, it is as likely for a parity-odd pion condensate to form as it is for a parity-even σ -meson condensate. This does not happen in nature, because nonzero quark masses break chiral symmetry explicitly, and thus favor a 0^+ condensate.

Similarly, it is important to add to the effective Lagrangian (19) terms which explicitly break the axial $U(1)$ symmetry:

$$\mathcal{L}' = -c \left(|\phi_1|^2 - |\phi_2|^2 \right) + m^2 |\phi_2|^2 \quad . \quad (21)$$

As shown by Berges and Rajagopal [4], the first term is due to instantons, with c proportional to the instanton density. Instantons are attractive in the $J^P = 0^+$ channel, and repulsive in the $J^P = 0^-$ channel, so c is positive.

In the second term, each power of the current quark mass m_q is accompanied by one power of ϕ_2^a . Since ϕ_2^a itself is not gauge invariant, the simplest gauge-invariant term is $m_q^2 |\phi_2|^2$ [1], so $m \sim m_q$. Thus, the pseudo-Goldstone boson for the axial $U(1)$ symmetry is extremely light, $m \sim 10$ MeV, taking m_q to be the up or down quark mass and assuming the constant of proportionality between m and m_q to be of order 1. This is in contrast to the explicit breaking of chiral symmetry, where the corresponding term is linear in the quark mass. The pseudo-Goldstone bosons are the pions which are relatively heavy, $m_\pi \simeq 140$ MeV $\sim \sqrt{m_q}$.

Both instanton and mass terms act to favor the formation of the 0^+ condensate ϕ_1 over that of the 0^- condensate ϕ_2 . Consider, however, the limit of very high densities. When the quark chemical potential $\mu \rightarrow \infty$, the instanton density and so c vanish like $\sim \mu^{-29/3}$ (for two flavors). The real question is whether at some density the current quark mass is negligible compared to the scale of the condensate. If this happens, we reach an ‘‘instanton-free’’ region in which quarks are effectively massless, \mathcal{L}' can be neglected, and parity is spontaneously broken.

Because mass terms are always present, the true thermodynamic ground state is always the parity-even 0^+ condensate, i.e., $\theta = 0$. There is, however, a finite probability for the system to condense in a parity-odd state, i.e., $\theta \neq 0$. The size and lifetime of this state is set by the mass of the pseudo-Goldstone bosons. For chiral symmetry breaking, the characteristic scale is $1/m_\pi \sim 1.4$ fm. This is small compared to the time and length scales of a heavy-ion collision, so that parity-odd fluctuations average to zero. On the other hand,

the region in space-time over which a parity-odd color superconducting condensate forms is large, $1/m \sim 20$ fm. If the collision time is shorter than this time scale, there is a finite probability that the system decays in a parity-odd state. We therefore propose to trigger on phase-space regions where nuclear matter is cool and dense, in order to observe the formation of parity-odd color-superconducting condensates on an event-by-event basis. A possible global parity-odd observable was discussed in [5].

REFERENCES

1. R.D. Pisarski and D.H. Rischke, nucl-th/9811104; nucl-th/9903023.
2. D. Bailin and A. Love, Phys. Rep. **107**, 325 (1984); M. Alford, K. Rajagopal, and F. Wilczek, Nucl. Phys. **B537**, 443 (1999); N. Evans, S.D.H. Hsu, and M. Schwetz, Nucl. Phys. **B551**, 275 (1999).
3. M. Alford, K. Rajagopal, and F. Wilczek, Phys. Lett. **B422**, 247 (1998); R. Rapp, T. Schäfer, E.V. Shuryak, and M. Velkovsky, Phys. Rev. Lett. **81**, 53 (1998); hep-ph/9904353; T. Schäfer and F. Wilczek, Phys. Lett. **B450**, 325 (1999); Phys. Rev. Lett. **82**, 3956 (1999); hep-ph/9903503 ; G.W. Carter and D. Diakonov, Phys. Rev. D **60**, 016004 (1999); K. Langfeld and M. Rho, hep-ph/9811227; M. Alford, J. Berges, and K. Rajagopal, hep-ph/9903502; D.T. Son, Phys. Rev. D **59**, 094019 (1999); E. Shuster, D.T. Son, hep-ph/9905448; D.K. Hong, hep-ph/9812510; hep-ph/9905523.
4. J. Berges and K. Rajagopal, Nucl. Phys. **B538**, 215 (1999).
5. D. Kharzeev, R.D. Pisarski, and M.H.G. Tytgat, Phys. Rev. Lett. **81**, 512 (1998); D. Kharzeev and R.D. Pisarski (in preparation).

5.3. D. Kharzeev: CP Violation in Au+Au?

It has been proposed by R. Pisarski, M. Tytgat and myself [1,2] that the discrete symmetries of strong interactions – parity \mathcal{P} and \mathcal{CP} – can be spontaneously violated in the vicinity of the deconfining phase transition. This would lead to a variety of dramatic effects which can be observed experimentally. What follows below is a brief and elementary introduction to the ideas of [1,2]. I refer the reader to these papers for all details and further references.

\mathcal{P} and \mathcal{CP} violation in strong interactions was never observed. However, in QCD, these symmetries cannot be taken for granted, and \mathcal{P} and \mathcal{CP} invariance should be regarded as a property of the ground state of the theory – the vacuum. When QCD vacuum is excited in a high energy nuclear collision, the properties of this excited vacuum state under \mathcal{P} and \mathcal{CP} transformations are in general not pre-determined, and will be defined by its structure. With these considerations in mind, let us recall briefly what is known at present about the \mathcal{P} and \mathcal{CP} symmetries of QCD.

Classical equations of motion of QCD are known to possess topologically non-trivial solutions – four-dimensional configurations of the gluon field which are characterized by different values of the “winding number” n . In this situation, the true vacuum of the theory should be represented as a linear superposition of states with different n ; this is analogous to the structure of the ground state in a crystal (Bloch wave function):

$$|\theta\rangle = \sum_n e^{i\theta n} |n\rangle, \quad (22)$$

where θ is called “ θ angle”, and n in terms of the gluon fields is defined as $n = \int d^4x Q(x)$, with the topological charge density $Q(x) = g^2/(32\pi^2) \text{tr}(G_{\mu\nu} \tilde{G}^{\mu\nu})$. Once an expectation value of a local observable is computed via the path integral, one has to include configurations of different winding numbers n with the weight given in (22). This procedure is equivalent to adding to the QCD Lagrangian a term

$$\mathcal{L}_\theta = \theta Q = \theta \frac{g^2}{32\pi^2} \text{tr}(G_{\mu\nu} \tilde{G}^{\mu\nu}). \quad (23)$$

Since in terms of the color electric, \vec{E} , and color magnetic, \vec{B} , fields, $G_{\mu\nu} \tilde{G}^{\mu\nu} \sim \vec{E} \cdot \vec{B}$, it is easy to see that the “ θ -term” (23) explicitly violates \mathcal{P} and \mathcal{CP} invariances if $\theta \neq 0$. \mathcal{P} and \mathcal{CP} conservation in QCD thus is not guaranteed *a priori*; however current experimental constraints on θ are very stringent, $\theta < 10^{-9}$, and this constitutes so-called “strong \mathcal{CP} problem”.

In terms of an effective theory of Goldstone bosons, the θ -term (23) manifests itself in the structure of the potential for the chiral $U(N_f)$ matrix. By a global chiral rotation, a constant U field can be rotated into a diagonal matrix. With $U_{ij} = \exp(i\phi_i) \delta^{ij}$, the effective potential can be written down as

$$V(\phi_i) = f_\pi^2 \left(-c \sum_i m_i \cos(\phi_i) + \frac{a}{2} (\sum_i \phi_i - \theta)^2 \right), \quad (24)$$

where the last term is proportional to the topological susceptibility, $a \sim \int d^4x \langle Q(x)Q(0) \rangle$ – the correlation function of topological charge at zero momentum, and m_i are current

quark masses. At zero temperature, the second term in (24) dominates, and the ground state is trivial, with $\langle \phi_i \rangle = 0$.

Based upon an analysis in the limit of a large number of colors, we suggested [1] that near the phase transition, a becomes much smaller than its value at zero temperature. In a mean field type of analysis, with T_d the temperature of the deconfining transition, and $t = (T_d - T)/T_d$ the reduced temperature, we found that $c(T) \sim 1/t^{1/2}$ and $a(T) \sim t$, so that the relevant ratio, a/c , scales as $a(T)/c(T) \sim t^{3/2}$. Once a/c gets small near T_d , the first term in (24) becomes comparable in magnitude to the second, and (24) admits non-trivial metastable vacuum solutions with $\sum_i \langle \phi_i \rangle \neq 0$. It is clear from (24) that non-zero values of $\langle \phi_1 + \phi_2 + \phi_3 \rangle$ act like having a system with non-zero θ -angle, $\theta \neq 0$. These solutions therefore correspond to metastable domains of \mathcal{P} - and \mathcal{CP} -odd vacua. Once the system is heated above the deconfinement phase transition and cools down, it can be trapped in one of these metastable \mathcal{P} - and \mathcal{CP} -odd states.

An obvious question is how this breaking of the discrete symmetry by a metastable bubble could be measured in nuclear collisions. As the bubble is odd under \mathcal{P} and \mathcal{CP} , the pions produced by its decay must also be in a state which is odd under these symmetries. For the collisions of nuclei with equal atomic number, as the initial state is even under \mathcal{P} , the observation of a \mathcal{P} -odd final state must be due to parity violation. In [1] we proposed measuring, on an event by event basis, a global variable which is odd under \mathcal{P} :

$$\mathbf{J} = \sum_{\pi^+, \pi^-} (\hat{p}_+ \times \hat{p}_-) \cdot \hat{z}, \quad (25)$$

where the sum includes all $\pi^+ \pi^-$ pairs in a given event, and \hat{z} is a fixed vector of unit norm. Various choices for this vector, as well as a general classification of \mathcal{P} -odd observables, can be found in [2]. Since the effective potential (24) is symmetric, \mathbf{J} on the average should vanish when summed over many events, and the distribution in \mathbf{J} should be symmetric with respect to zero. \mathcal{P} -odd effects therefore will manifest themselves in a non-zero width of this distribution.

It is easy to understand why \mathcal{P} -odd bubbles induce non-zero values of \mathbf{J} in a given event. In terms of the underlying gluonic fields, the \mathcal{P} -odd bubbles arise from fluctuations in the topological charge density, $G_{\mu\nu} \tilde{G}^{\mu\nu}$. Consider the propagation of a quark anti-quark pair through a region in which $G_{\mu\nu} \tilde{G}^{\mu\nu} \sim \vec{E} \cdot \vec{B} \neq 0$. If \vec{E} and \vec{B} both lie along the \hat{z} direction, then a quark is bent one way, the anti-quark the other, so that $(\vec{p}_q \times \vec{p}_{\bar{q}}) \cdot \hat{z} \neq 0$, where \vec{p}_q and $\vec{p}_{\bar{q}}$ are the three-momenta of the quark and anti-quark, respectively. An estimate of the effect can be done by considering the topologically non-trivial solutions directly in terms of collective pion fields [2]; we find that the \mathcal{P} -odd asymmetries can be relatively large, at least $\sim 10^{-3}$. \mathcal{P} and \mathcal{CP} violation in nuclear collisions is therefore possible, and should be searched for.

REFERENCES

1. D. Kharzeev, R.D. Pisarski and M.H.G. Tytgat, Phys. Rev. Lett. 81 (1998) 512.
2. D. Kharzeev and R.D. Pisarski, hep-ph/9906401.

6. M. Gyulassy: Concluding Remarks

We have seen considerable variation in section one on the predictions of global observables (Bass, Bleicher, Cassing, Drescher, Eskola, Wang). Much of the factor of two uncertainty in the initial entropy and transverse energy are inherent our ignorance of the initial conditions and especially its soft component. However, as emphasized by Eskola and Wang a large part of that uncertainty is also due to interesting controllable physics. That component, nuclear shadowing and anti-shadowing of the structure functions, can in fact be inferred from systematic $p + A$ studies at RHIC (Wang, Lin) or in $e + A$ when electron beams can eventually be aimed through RHIC (Kovchegov). The $p + A$ experimental studies are **mandatory** prerequisites not only to reduce the uncertainties in the initial conditions at RHIC, but also from the fundamental goal of simply understanding the nuclear wavefunction on the light cone. At first, light ion data, e.g. $Si + Au$, will be essential to get a feeling for the size of those effects, but eventually a full complement of pp and pA data will be needed as at the AGS and RHIC to untangle the physics.

The A,B dependence of asymmetric systems as well as multiplicity dependence is also key to understanding the deviations from phase space saturation. Fireball models as shown in section 2 suggest that hadro-chemical equilibration is approached in strangeness to a surprising degree, and most microscopic models cannot reproduce the observation without invoking novel concepts such as baryon junctions (Vance) and higher Casimir flux tubes (Sorge). However, the linear variation of $\langle K \rangle / \langle \pi \rangle$ with multiplicity in NA49 for example suggests that nonequilibrium effects play an important role. Deviations from flavor equilibration predicted by Stachel will also be important to look for at RHIC. Those deviations can provide us a handle to learn about the physics of dense matter. They may be due to phase space coalescence (Zimanyi), small relevant transport cross sections, or interesting medium mass modifications near the chiral symmetry boundary (Rapp, Schaffner). Just as the interesting physics are deviation from OSCAR certified [3] transport theories, the deviations from fireball fits must be carefully scrutinized as emphasized by Rafelski.

I cannot over emphasize enough the importance of gaining control over the initial conditions. As Schlei and Dumitru pointed out, the data can be fit with almost any transport or hydro model is we are allowed the freedom to dial in arbitrary initial condition. The goal of the RHIC program is however not to tabulate arbitrary initial conditions but to understand in detail the energy and A dependence of the initial as well as the final conditions. Only with knowledge of the initial conditions can we interpret collective observables such as directed, transverse, and azimuthal asymmetric flow and such as possible time delay via HBT as evidence for new physics.

One collective probe emphasized by Dumitru from the hydrodynamic point of view is dE_{\perp}/dy that decrease in general if work is done by the system. However, given the present uncertainties in the absolute height of "Mount RHIC", I suggest that the following simpler relative measure of longitudinal collectivity:

$$R(\tau) = dE_T/d\eta/dN_{ch}/d\eta$$

Since Bjorken's work, it is known that an ideal $p = \epsilon/3$ equations of state leads to $R(\infty)/R(\tau_0) \sim 1/2$ due to pdV work associated with longitudinal Bjorken expansion.

Covariant transport theory as discussed by Zhang and Molnar predicts less but still significant longitudinal work $R(\infty)/R(\tau_0) \sim 3/4$, due to finite size dissipation.

One of the most interesting observations at the SPS in my opinion was in fact **NO** evidence for any longitudinal work. Both E_{\perp} and N_{ch} are observed to scale almost perfectly with the number of wounded nucleons. Models such as RQMD and UrQMD provide a possible answer to the missing work puzzle. Heavy resonances and strings in such models mimic the mixed phase in QCD where the speed of sound is anomalously small. The mixed phase is notoriously lazy, as Hagedorn taught us! Excitation energy is wasted making heavy resonances instead of converting into collective motion. At RHIC, much higher initial energies are expected to be produced via mini-jets than at SPS, well into the plasma phase. There the speed of sound is expected to approach $1/\sqrt{3}$ again, the freshly produced plasma can push its neighboring cells more efficiently down the beam pipe with a resulting in decreasing R .

It is important to distinguish this type of collectivity from that observed associated with radial and elliptic flow and discussed in section 3. Those may also be sensitive to interesting variations in the equation of state. However, the longitudinal work occurs mostly during the early times when the longitudinal gradients $\sim 1/\tau$ are the largest. Transverse collectivity may develop over longer times because the transverse gradients are $\sim 1/R_A$. The system must spend its first three fm deep in the plasma phase to get longitudinal work going. At the SPS lazy mixed phase produces no significant longitudinal work. Note that the hadron systematics in section 2 indicate that AA at those energies cross the transition region but the simplest signal of longitudinal collectivity was not seen. So my prediction is that we will start to see R decrease for the first time at RHIC as a function of centrality and A.

One of the most exciting new frontiers at RHIC is high p_{\perp} nuclear physics (see Eskola, Wang, Vitev, Snigirev, Srivastava). Unlike at SPS, where much theoretical ambiguity in pQCD results from uncertainties associated with intrinsic k_{\perp} smearing as discussed by Wang, at RHIC collider energies the pQCD power law tail is predicted to stick out clearly. This provides a calculable, reliable base or calibration point from which deviation can be used to extract the physics of dense matter. In Fig. 34 from [1] the contrast between the now known SPS and the predicted RHIC domain is evident. At the SPS HIJING accidentally fits the data, but variations of uncontrolled soft hadronization assumptions leads to extreme discrepancies. At RHIC on the other hand, that soft component has much smaller influence on the high $p_{\perp} > 3$ GeV domain. Therefore it becomes possible to look for new physics such as the non-linear energy loss of gluons predicted by BDMSP. The magnitude of predicted jet quenching phenomena is illustrated in the figure.

Heavy flavor physics at RHIC will also be interesting as emphasized in section 4. The open questions left by NA50 can be clarified at RHIC energies which is well above the charm thresholds and the high energy densities occur already in much smaller A systems. The anomalous J/ψ deficit has been predicted to occur by Satz already in $Cu + Cu$, and brand X comover alternative scenarios will be much more easily ruled out as emphasized by Vogt. The topic of open charm is also rich with speculation and possibilities as discussed by Lin and Thews.

Finally, I comment on section 5. The predictions for truly exotic and novel dynamics associated with chiral restoration, P violation at high baryon densities and especially

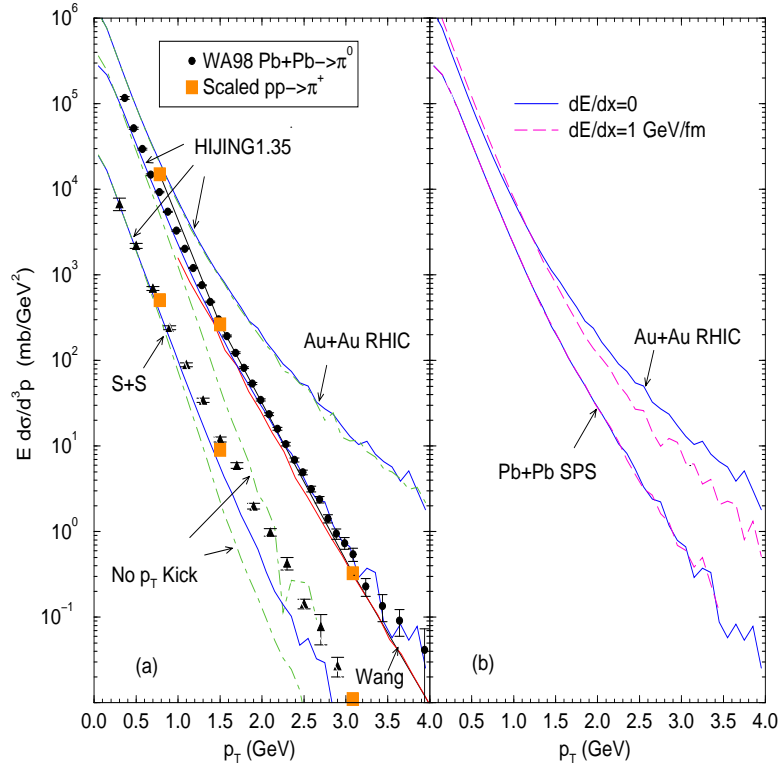


Figure 34. Opening of the high p_{\perp} window at RHIC from [1]. a) The WA80 $S + S$ data (triangles) and the WA98 $Pb + Pb \rightarrow \pi^0$ data (dots) are compared to HIJING1.35 with soft p_{\perp} kicks (full lines) and without p_T kicks (dot-dashed curves). The later scale with the wounded projectile number times σ_{AA} times the invariant distribution calculated for pp . The parton model curve from X.N.Wang is labeled by 'Wang'. The filled squares show $pp \rightarrow \pi^+$ data scaled by the (Glauber) number of binary collisions times σ_{AA} for both SS and $PbPb$. b) Significant jet quenching predicted for RHIC energies [2], is masked by soft physics at SPS energies in the HIJING model.

possible CP violating domains add great excitement to exploratory experiments at RHIC. While the predictions are based on very bold and even further extrapolations from known physics than those discussed in the previous sections, those directions associated with subtle many-body quantum phenomena should also be pursued vigorously because the potential payoff is so high.

REFERENCES

1. M. Gyulassy and P. Levai, Phys. Lett. B442 (1998) 1.
2. X.-N. Wang and M. Gyulassy, Phys. Rev. Lett. **68**, 1480 (1992).
3. Y. Pang, <http://rhic.phys.columbia.edu/>,
OSCAR II, <http://thy.phy.bnl.gov/www/riken/oscar2.html>.